AN ABSTRACT OF THE DISSERTATION OF

John Gamble for the degree of Doctor of Philosophy in Biochemistry and Biophysics presented on December 6th, 2018.

Title: Analysis of Cancer Progression by Establishing Quantitative Assessments of Zebrafish Xenografts

Abstract approved:

_____

Julie A. Greenwood

The goal of this dissertation was to improve our abilities in acquiring critical *in vivo* data by establishing embryo-larva zebrafish as an exemplary model to quantitatively evaluate cancer progression. The living environment that encompasses a tumor has a significant effect on how cancer develops, grows and metastasizes. In order to study cancer, we must observe it in this influential environment. Zebrafish embryo-larva provide a vertebrate anatomy that provides a window into how cancer cells behave. In this dissertation, I demonstrate how embryo-larva zebrafish can be utilized to study glioblastoma cell progression, how to capture and quantitate those aspects of progression and how they can be used to effectively evaluate potential cancer therapeutics.

Presented in this work are three chapters of original work with the second and third being published and the fourth comprising both published and soon to be published work. The second chapter of this dissertation examines laminin alpha 5's, an extracellular matrix protein, effects on glioblastoma progression. By using embryo-larva zebrafish for xenografts, we determined laminin alpha 5 impaired glioblastoma invasion throughout the brain and encouraged microtumor formation. With this work, we were the first to demonstrate laminin alpha 5's effect on glioblastoma in an *in vivo* setting, which were contrary to what was observed *in vitro.*

Furthermore, we designed methodology for others to examine cancer invasion and progression using zebrafish and freely available image analysis software.

In the third chapter, I present commentary and methodology for quantitatively analyzing cancer cell invasion in a 4D environment. Within this chapter, I present methods for using ImageJ/Fiji software to track cancer cell movement and provide 3D time-lapse data. Additionally, I present quantifiable attributes to describe and measure cancer cell invasion that can be taken from the cell tracking data. This work was published with Microscopy and Microanalysis in conjunction with a poster that was presented at their annual 2017 conference which went on to win the top prize in its category that day.

For the fourth chapter of this dissertation, several potential cancer fighting drugs are tested on various cancer types using zebrafish xenografts. All tested drugs take advantage of the pro-survival protein, Bcl-2, where they bind and alter its conformation into a pro-death protein. The chapter is composed of three sections where the first section demonstrates a peptide's, NuBCP-9, ability to induce apoptosis in chemotherapy resistant lung cancer cells in a Bcl-2 dependent manner. The second section establishes a nanoparticle light-based delivery system for the peptide where we successfully reduce growth on chemotherapy cancer cells in zebrafish xenografts. Lastly, in the third section, we test a number of small molecule drugs for their effectiveness in treating chemotherapy resistant lung cancer and triple negative breast cancer in zebrafish xenografts.

Finally, in my fifth chapter, I discuss some noteworthy insights gained while conducting zebrafish xenograft experiments.

Analysis of Cancer Progression by Establishing Quantitative Assessments of Zebrafish Xenografts

by
John Gamble

A DISSERTATION

submitted to

Oregon State University

in partial fulfillment of
the requirements for the
degree of

Doctor of Philosophy

Presented December 6th, 2018
Commencement June 2019

Doctor of Philosophy dissertation of John Gamble presented on December 6, 2018

APPROVED:

Major Professor, representing Biochemistry and Biophysics

Head of the Department of Biochemistry and Biophysics

Dean of the Graduate School

I understand that my dissertation will become part of the permanent collection of Oregon State University libraries. My signature below authorizes release of my dissertation to any reader upon request.

John Gamble, Author

ACKNOWLEDGEMENTS

First, I would like to thank my co-mentor, Julie Greenwood, for taking me into her lab and giving me great opportunities to flourish in my work. You grew my passion for cell biology and the microscopy techniques to study it. I am grateful for her mentorship and all the great advice she would provide me (even if I did not always follow it and regretted it later). I would like to thank her for all her patience and encouragement as I developed as a scientist and learned how to progress my ideas into action.

Thank you as well to my other co-mentor, Siva Kolluri. I greatly appreciated our collaborations that provided opportunities for me. Thank you for accepting me as a member of your lab and providing me avenues to contribute. While working with Siva, he was always willing to give a friendly ear and provide a boost when needed. I must also thank all of my fellow Kolluri Lab members Hyo Sang Jang, Martin Pearce, Jessica Phillips, Bach Nguyen, Veronica Puig Sanvicens, Daniel Elson and many others. They always made me feel welcome and were always eager to help and provide feedback on projects. Thank you, in particular, to Martin Pearce for being a great person to collaborate with and working hard to make great science. My third chapter would not be possible without the work you contributed to it.

My work could not have been done without the SARL facility and the people who run it. In particular, I would like to thank Jane La Du for her help early on in my career in teaching me many techniques and getting me started with zebrafish. A big thank you to Carrie Barton and the fish room as well. Carrie was always so helpful in providing zebrafish embryos, even when I needed zebrafish last minute. Also, I cannot forget to thank Robert Tanguay for his advice and help with editing many of my works. Thank you for permitting me attend and contribute to your lab meetings as they were a valuable experience.

Additionally, my work could not have been possible without the confocal microscope maintained by the CGRB. In particular, thank you to Anne-Marie Girard Pohjanpelto for training me on all the various aspects of the confocal microscope and

all her help in keeping the microscope running and available. It feels like I spent half my career in the confocal room and I rarely had an issue.

I would also like to thank all the many undergraduate students that occupied the Greenwood lab while I was at Oregon State, Yuriyah Reed-Harris, Kayla Stalheim, Christine Kang, Sophie Means, Arisa Larmay Barrientos, Alexis Murphy and Dominique Holman. I was a pleasure working with you all in the lab. I first learned how to do zebrafish xenografts under Kayla's direction. Many thanks to Yuriyah for helping me with the work to publish the paper entailed in chapter three and thank you for being a fun fellow lab mate to work with. Also, thank you to Leah Wehmas for giving me a starting point of which to begin my work.

Lastly, I must thank my family for supporting through this Ph.D. journey. My parents have always provided me with confidence and encouragement that I can do anything. I appreciate them and my sister for understanding my need to travel so far away from Georgia to pursue my degree and new experiences. Most of all, thank you to my wonderful wife, Rachel. I could write an entire additional dissertations worth of pages detailing all my gratitude and thankfulness for having your support and help in completing my degree. I would truly be lost without.

P.S. No thanks to my two dogs Beau and Lola, while cute and loveable they have been a burden throughout the entire process and in no way assisted in my endeavors.

CONTRIBUTION OF AUTHORS

Chapter 2: All data was collected and analyzed by John Gamble unless otherwise noted. Yuriyah Reed-Harris contributed in RNA extractions, gel electrophoresis, and imaging of zebrafish xenografts. Xenografts were done by John Gamble. Cell cultures were maintained by John Gamble and Yuriyah Reed-Harris. Jane La Du and Carrie Barton helped provide critical advice and help with morpholino microinjections. John Gamble and Julie Greenwood helped with experimental designs. All text was written by John Gamble with edits from Robert Tanguay and Julie Greenwood.

Chapter 3: All text was written by John Gamble with edits by Robert Tanguay and Julie Greenwood. Methodologies were created by John Gamble.

Chapter 4: Experimental designs were done by Martin Pearce, Siva Kolluri, Erin Morgan, Norbert Reich and John Gamble. Molecular biology experiments were conducted by Martin Pearce, Erin Morgan and John Gamble with Martin Pearce contributing the majority. Cell-based experiments were conducted by Martin Pearce and Erin Morgan. Cell cultures were maintained by Martin Pearce, Erin Morgan and John Gamble. Zebrafish xenograft experiment were conducted by John Gamble. John Gamble, Martin Pearce and Erin Morgan contributed to data analysis. Robert Tanguay generously supplied zebrafish. Text was written by John Gamble, Martin Pearce and Erin Morgan with edits by Siva Kolluri and Norbert Reich.

TABLE OF CONTENTS

TABLE OF CONTENTS (Continued)

Page

TABLE OF CONTENTS (Continued)

Page

LIST OF FIGURES

Figure Page

LIST OF FIGURES (Continued)

Figure Page

LIST OF TABLES

Chapter 1: Introduction

Author: John Gamble

1. 1 Drug Testing using Zebrafish Xenografts

1.1.1 Zebrafish as an In Vivo Model

Drug discovery requires both *in vitro* testing on human cell cultures and *in vivo* experimentation in animal models. Cell culture provides the ability to screen numerous potential therapies rapidly on many different cancer types. However, a homogeneous collection of tumor cells in a 2D environment have little relevancy to actual tumor biology in humans. For instance, breast cancer cell lines cultured in 3D cell cultures can have different expression and post-translational states for important drug targets such as epidermal growth factor receptor, human epidermal growth factor receptor 2 and pAKT when compared to 2D cell cultures [1]. Additionally, the environment surrounding cancer cells provides countless physical and biochemical pressures that influence their development and susceptibility to drugs. The extracellular matrix is a collection of proteins, glycoproteins, proteoglycans and polysaccharides that create a barrier between the tumor and healthy tissue, but also provide a network of adhesion sites and retain an abundance of signaling factors [2]. Attachment to the extracellular matrix that surrounds tumors can confer resistant to chemotherapy treatments by suppressing chemotherapy induced apoptosis as well as inducing malignant behavior [3,4]. Integrin receptors on cancer cells can bind specific proteins in the extracellular matrix and transduce survival and migration activity signaling [3,5]. Animal models are needed to provide a more accurate tumor environment in order to correctly test cancer therapeutic drugs. While the gold standard for *in vivo* experimentation has been the mouse model, high expenses in animal maintenance and procedures negates experimental testing of many potential drugs. Additionally, upper level vertebrate animals, like mice, have stringent animal care policies that prevent or limit the scope of drug testing. Moreover, complex procedures and the long time-frame of experiments, make high-throughput testing impossible. Zebrafish may offer a much-needed stepping stone in translating *in vitro* to *in vivo* results that also provides high-throughput capabilities.

Zebrafish (*Danio rerio*) are small tropical freshwater fish that have become a model organism for studying animal development, toxicity and human diseases. Zebrafish offer many advantages as an animal model for human cancer study.

Zebrafish have high fecundity and develop rapidly. Mating can yield hundreds of fertilized eggs that within days develop into embryos with formed organs [6]. At this young age, zebrafish embryos are transparent allowing non-invasive observation inside the animal. Due to their small size and aquatic nature, they are relatively inexpensive to maintain, allowing researchers to keep thousands of fish in a laboratory. While not mammals, zebrafish have a comparable vertebrate anatomy to humans and have orthologs for 70% of human proteins with 82% of them being disease causing [7]. With recent developments in technology, zebrafish are relatively easy to alter transcriptionally and genetically. Morpholino oligonucleotides can be injected into fertilized single cell eggs to silence complementary mRNA to suppress specific protein translation in early zebrafish development [8]. Alternatively, with CRISPR Cas9 technology the zebrafish genome can be edited to effectively knock out proteins or insert new genes leading to an ever-growing list of transgenic models [9]. These attributes can provide researchers valuable tool with the flexibility to answer many different cancer biology questions, including cancer drug discovery.

1.1.2. Zebrafish Xenografts

Xenograft transplantation is the relocation of living cells from one species to another. Research by Lee., *et al* demonstrated zebrafish are an advantageous model to for human cancer cell transplantation [10]. The transplanted human cells not only survived but were able migrate and interact with the host environment. Subsequent zebrafish xenograft experiments also resulted in successful engraftment with various other human cancer lines, such as those from breast and leukemia, and demonstrated capability of tumor formation [11–14]. The embryo-larva zebrafish offers a number of advantages over other xenograft models (Figure 1.1). At the young age, zebrafish lack an adaptable immune system and thus remove the need for immunosuppressive drugs or immunocompromised variants [15]. Moreover, the zebrafish are millimeters in size and therefore can be kept in petri dishes or individually in 96-well plates. Despite zebrafish preferring an environmental temperature of 28^{o}C, they are capable of surviving at temperatures from 32 to 36^{o}C, much closer to human conditions [15–17]. Additionally, zebrafish transplantation requires far few cancer cells than rodent models. Zebrafish transplantations require only hundreds cells or fewer while mouse

xenografts require several times as many [18]. This is of particularly importance when cancer cell numbers are finite, such as with primary patient tissue samples. Furthermore, within a couple of days post fertilization, zebrafish embryos provide a complement of orthotopic organs and tissues such as the brain, heart and liver as well as a functioning circulatory system [6,19].

Zebrafish offer accessibility to researchers needing *in vivo* testing as they provide relatively low cost of maintenance and care. Moreover, zebrafish deliver a model where cancer progression can be assessed by imaging equipment available to most researchers, such as standard epifluorescence and confocal microscopes. Due to the transparent nature of embryo-larva zebrafish, assessment of potential drug success can be done non-invasively within the host. Transparent zebrafish tissue provides extraordinary optical penetration allowing researchers to collect detailed images of fluorescent cancer cells. With the organism's tissue thickness in the micron scale, excitation/emission spectrums of fluorescent probes escape the tissue with little light scattering, particularly at longer wavelengths. Fluorescent proteins such as mCherry and GFP and fluorescent dyes like CM-DiI and CMFDA have been successfully used to not only visualize individual cells in zebrafish, but also subcellular structures, i.e. centrosomes, endosomes, mitochondria, microtubules, etc. [20–23].

Researchers have discovered that the zebrafish yolk provides a simple *in vivo* environment for human cancer cells to proliferate and migrate [18]. At the embryonic and larval stages, zebrafish rely on their yolk to supply them with the necessary nutrients to grow and develop. The yolk provides a nutrient rich environment hospitable to engrafting hundreds of cancer cells. The yolk sac's size aids in the transplantation process as it provides a relatively large injection site that is easy to identify and transplant into with a microinjector. Many different human cancer cell lines, i.e. breast, neuroblastoma, melanoma, leukemia, prostate and ovarian cancers, can survive and proliferate in the zebrafish yolk [18]. With transplantation into the yolk, many different cancerous abilities can be assessed with the most predominate being growth-survival, invasion and metastasis potential (Figure 1.2). Cancer cell proliferation can be prolific as malignant cells can quadruple in 3 days while inside the zebrafish yolk [11]. Aggressive cancer cells can quickly migrate and exit the yolk

sac by entering the blood stream to travel throughout the body [24]. Moreover, transplanted patient-derived gastrointestinal tumor cells were capable of forming micrometastases in zebrafish unlike non-tumor cells that were also transplanted [12]. Moreover, zebrafish xenograft experiments have replicated results done in mouse xenografts where breast, prostate, colon and pancreatic cancer cell lines that metastasized in mice also metastasized in zebrafish, while non-metastasizing cell lines did not [25].

Blood vessels are an integral part of tumor development. Zebrafish have been used to measure tumor cell and blood vessel interactions. To simulate blood vessel growth, tumor cells secrete angiogenetic factors [2]. With transgenic zebrafish like Tg(fli:EGFP)^{y1} zebrafish with GFP expressing vascular endothelial cells, researchers can study cancer induced angiogenesis [11,26]. Within 24hrs of implantation, angiogenesis can be measured as zebrafish blood vessels can be seen growing towards transplanted human tumor cell masses [11,26,27]. Additionally, the zebrafish blood vessels offer the necessary architecture to access metastatic characteristics, like extravasion and intravasion, of tumor cells. With metastatic cancers, cancer cells must enter, intravasion, into the blood stream and exit, extravasion, back out in order to travel to other organs and tissues [28]. Tumor cells transplanted into the blood stream of zebrafish are capable of extravasion as tumor cells can be seen attaching to the endothelium and exiting the capillaries [5]. Intravasion can also be seen as tumor cells transplanted into the yolk can invade into the blood stream, travel to the tailfin and form micrometastasises [25].

While the zebrafish is missing some human relevant organs, i.e. lungs, breast, orthotopic transplantation is possible for a number of cancers with brain being the most widely used. The brain is developed with fore-, mid- and hindbrain ventricles by the end of the zebrafish embryonic stage [6]. These ventricles provide a pocket for cancer cells to occupy. The larval zebrafish brain provides a complex environment with glia, neurons and blood vessels are held together by a unique ECM [29–31]. A functioning vasculature permeates the brain as well, where pericytes and endothelial cells provide a basement membrane and protective blood brain barrier by 4-day post fertilization [32]. Transplanted human glioma cells in a zebrafish brain environment

exhibit behavior seen in human patients as cells aggressively invade the surrounding tissue while migrating and along cranial blood vessels [17]. Furthermore, to maneuver through the environment, glioblastoma cells can be seen transitioning between amoeboid and mesenchymal type mechanisms to squeeze and pull through the tight spaces in the brain [29,33].

1.1.3. Testing Cancer Therapeutics

While drugs may be effective and efficient at killing or hindering cancer growth *in vitro,* they might cause complex problems in multicellular systems. Rodent models are the standard for toxicity testing, but they are too expensive and impractical for early drug testing. In an effort to cover this gap, embryo-larva zebrafish have established themselves as a sensitive and predictive model for human toxicity. Humans and zebrafish share similarities in embryogenesis with conserved gene expression across phyla as well as many anatomical and physiological features being developed [34]. During the pharyngula stage of development, both mouse and zebrafish development correlate with measured transcriptomes [35]. Systemic toxicity can be quickly assessed as treatments are added directly to the fish media. Toxic effects can be seen in zebrafish survivability, but also with defined developmental phenotypic abnormalities that can arise [36]. Malformations, such as edemas, can provide insight into mechanisms of drug toxicity to aid in modification of drug design. This may serve to help researchers in designing the most efficient drugs with limited toxicity.

The embryo-larva zebrafish's diminutive size is highly conducive to cancer drug screening. Being aquatic animals, zebrafish must be maintained in a salt buffered water medium. With their small size, single or multiple zebrafish can be stored in 96-well plates during the embryo-larva stage. The 96-well format aids in the ability to quickly and easily treat with multiple concentrations of different small molecules. Additionally, small molecules are absorbed freely into the fish and reach their target with minimal interference from epithelial barriers or metabolic enzymes, allowing researcher to focus on drug biological processes [37]. Furthermore, each embryo-larva requires a small volume of media and therefore treatment can be accomplished with minimal quantities. Moreover, the entire fish can be captured with a wide-field

objective allowing for rapid acquisition of phenotypic effects. Using high-content microscopes, this process offers the ability to collect data on large numbers of xenografts [38,39].

There are currently a couple different methods to assess differences in cancer growth with zebrafish xenografts (Figure 1.3). For both methods, fluorescent cancer cells are transplanted into embryonic zebrafish and allowed to develop over several days. One method requires sets of zebrafish be sacrificed before and after treatment and enzymatically dissolved to produce a unicellular suspension [11,40]. Fluorescent cells are then fixed and counted on a hemocytometer or flow cytometry to compare between treatment groups. Sacrificing and counting cells provides an accurate count of the number of cells and therefore can provide a more accurate proliferation rate. Additionally, with other staining procedures, living and dead cells can be counted as well as protein expression levels using fluorescent antibodies. However, due to animal sacrificing there can no longer be a comparison of time points for each animal and therefore rely must rely on less statistically powerful unpaired group comparisons [41]. This is of importance as each zebrafish xenograft will have a different number of transplanted cells due to injection error. Because zebrafish xenograft transplantations engraft a small population of cells, slight variations in transplantation numbers can result in large percent differences between xenografts. Disproportionally sacrificing xenografts with low/high cell numbers before treatment could skew calculated proliferation rates. Furthermore, this method is labor intensive and therefore limits the capability for screening many potential drugs. For the other method, instead of animal sacrificing, images of the fluorescent cells in the zebrafish are taken before and after treatment [16,17,42]. Differences is fluorescent cell area and intensity can be used to measure cancer growth. By imaging the cells within the zebrafish, direct comparisons can be made within each animal. This results in a more powerful statistical paired test and higher *N* value. Additionally, high-content imaging microscopes can be used to help automate the process, giving the capability for high-throughput. However, cells cannot be counted individually as they are typically indistinguishable in a large mass. Changes in area and intensity are relied upon for growth information and while increases in both can be correlated to cancer growth,

they cannot be directly correlated to cell proliferation rate. Approximations can be made based on average cell size, but this falls short of an absolute cell count. As a result, fold changes in cell growth can have large variations as doubling in cell numbers can equate to 4 or more times larger area/intensity values. Furthermore, determining living and dead cells as well as cancer protein expression is not possible *in vivo,* and zebrafish must be dissolved or fixed whole for staining or immunohistology.

Cancer invasion and migration are correlated to a cancer's ability to metastasize. Approximately 90% of all cancer deaths are due to metastasis [43]. Cancer therapeutics that can limit cancer cell motility are of great value as they can reduce the spread of the disease and increase the life of patients. Migration and invasion of cancer cells can be captured in zebrafish embryo-larva. Since cancer cells can be seen throughout the body of the translucent embryo-larva zebrafish, cancer cells that have left the transplantation site can be seen and accounted for. Metastatic cancer cell lines, like MDA-MB-231, disperse throughout the zebrafish days after transplantation where differences in metastatic potential can be measured by the percentage of zebrafish with invasive cells or by the average number of invasive cells [25,44,45]. Additionally, dispersal of cells can be measured locally within a tissue, such as the brain. With increased magnification, dispersal distances can be measured for individual cells. Our lab has demonstrated the ability to measure significant differences in cell invasion within the zebrafish brain [17,42]. Furthermore, a cancer's metastasis ability can be accessed further by identification of micrometastases. Studies have shown cancer cells leave the yolk sac and extravasate into the perivascular tissue where they establish micrometastases [12,46].

1.1.4 Challenges with Zebrafish Xenografts

There are challenges that remain for zebrafish to reach their full potential as a human cancer model. To obtain consistent images of fluorescent transplanted cancer cells, zebrafish must be manipulated into a standardized position close to the microscope objective. This is particularly difficult for brain xenografts as zebrafish must be positioned dorsal side down so that the brain is not obstructed from the animal's large eyes. Manual manipulation of zebrafish in a medium, such as low

melting point agarose, remains the most common positioning method. While providing consistency, the process is slow and labor intensive. Positioning becomes more difficult as zebrafish embryo-larva develop swim bladders and become difficult to position at the bottom of the well. While researchers have created tools such as 3D printed designs to create better topography for zebrafish body orientation, these methods still rely on manual manipulation. In an effort to create true high-throughput capabilities for zebrafish, capillary imaging systems have been designed to automatically extract embryo-larva zebrafish, image and re-place them. While a capillary imaging system offers automation, the lack in speed prevents large numbers of embryos-larvae from being imaged as each individual zebrafish is manipulated and imaged. The VAST BioImager™, a commercially available system, claims imaging times of 50 sec/zebrafish [47]. With different treatment media as a concern, wash steps in between zebrafish would require significantly more time. Quickly proliferating or migrating cells could cause problems in consistency between zebrafish groups as imaging time increases.

Another challenge for the zebrafish xenograft cancer model is the xenograft procedure. Cancer cell transplantation can be a limiting factor for zebrafish xenograft experiments. As with imaging, current transplantation methods require manual manipulation of the zebrafish embryo-larva but also skill to inject consistent numbers of cancer cells. While yolk transplantation offers less difficulty in the transplantation process than other locations, individuals must be highly trained to preform microinjections as human cells can be difficult to deliver a consistent number of cells into the zebrafish. Currently, zebrafish xenograft procedures are done using an air-driven pressure microinjector that uses a pulled glass needle. With proper training, an individual can inject hundreds of zebrafish embryo-larva per hour with less than 5% casualties, however, training is not trivial as individuals must be capable of quickly manipulating small zebrafish embryo-larva and injecting cancer cells with minimal harm to the animal. Moreover, cancer cells do not disperse evenly throughout the needle and can easily clog the needle due to cell-cell contacts. Additionally, cancer cell types have varying characteristics, i.e. size and cell-cell contract propensity, adding increased challenges when testing multiple cancers.

Rapid developmental time for zebrafish also present a potential problem for investigators. While quick development is advantageous in providing an animal with developed organ systems, it also limits assay capabilities. Early in development, zebrafish embryo-larva can sufficiently survive on their yolk without intaking other food. However, this developmental period is short lived and therefore limits assay potential to a 3 to 4-day period. With slower growing cancers, differences in growth may not be realized. This could particularly hamper attempts to utilize patient derived tumor tissue as the tumor cells may not establish or grow quickly as they are a heterogenous collection of cancerous and non-cancerous cells unlike homogenous immortalized cancer cell lines. Additionally, treatments must have a quick, robust effect to display a significant result on transplanted cancer cells. While signs of apoptosis can be displayed within hours for cells in culture after treatment with a chemotherapy, cells within tissue may take days before features of apoptosis is perceived [48–50].

1.1.5 Conclusions

With simplistic *in vitro* environments, researchers can efficiently test new cancer therapeutics. However, there is increasing evidence that limits the usefulness of cancer cell behavior *in vitro*. [2,51]. Zebrafish offer a vertebrate anatomy with a hospitable *in vivo* environment containing relevant structures, i.e. ECM and flowing blood vessels, necessary for human tumor development [17,26,52]. Moreover, zebrafish are economical *in vivo* models for early drug testing and provide researchers the capability to test effectiveness and toxicity of potential drugs before committing to testing in rodent models. Furthermore, zebrafish provide the capability for high-throughput testing, in contrast to rodent models. As technology and methodology advance, zebrafish have the potential to become a vital part of cancer drug discovery by providing bridge for translation of studies *in vitro* to *in vivo.*

1.2 Figures

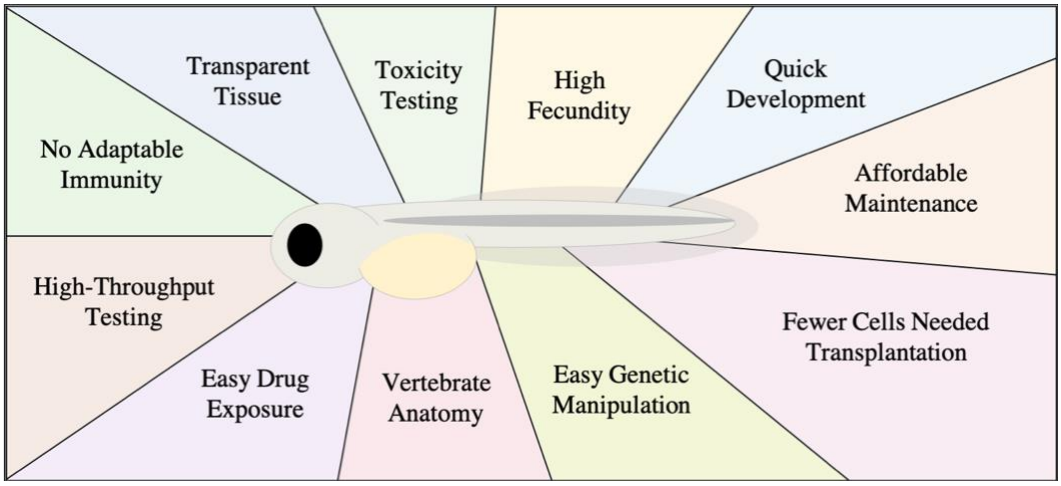

Figure 1.1. Diagram of advantages for using a zebrafish xenograft model.

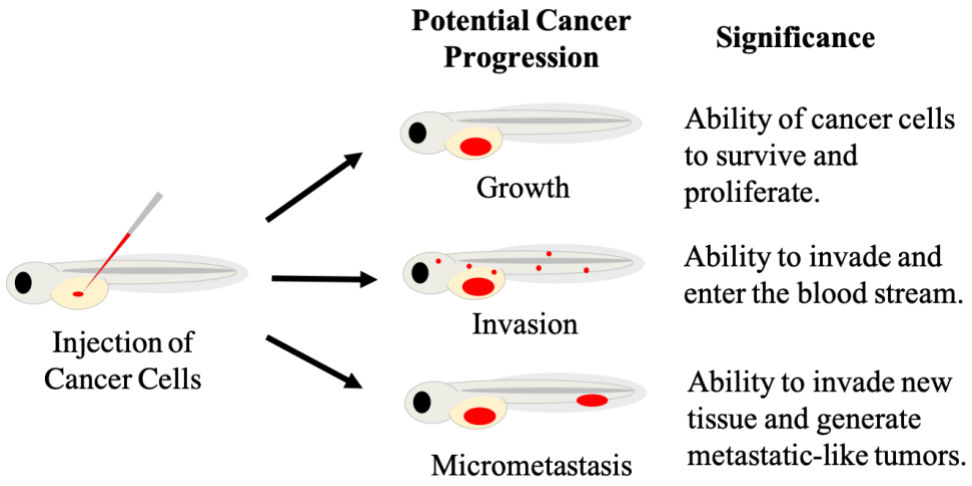

Figure 1.2. Diagram depicting measurable signs of cancer progression in zebrafish xenografts. Human fluorescent cancer cells (red) are injected into the yolk of embryonic zebrafish (left). Cancer progression can display as growth, invasion or micrometastases (center). These phenotypic responses can be measured to provide information on specific cancer behavior.

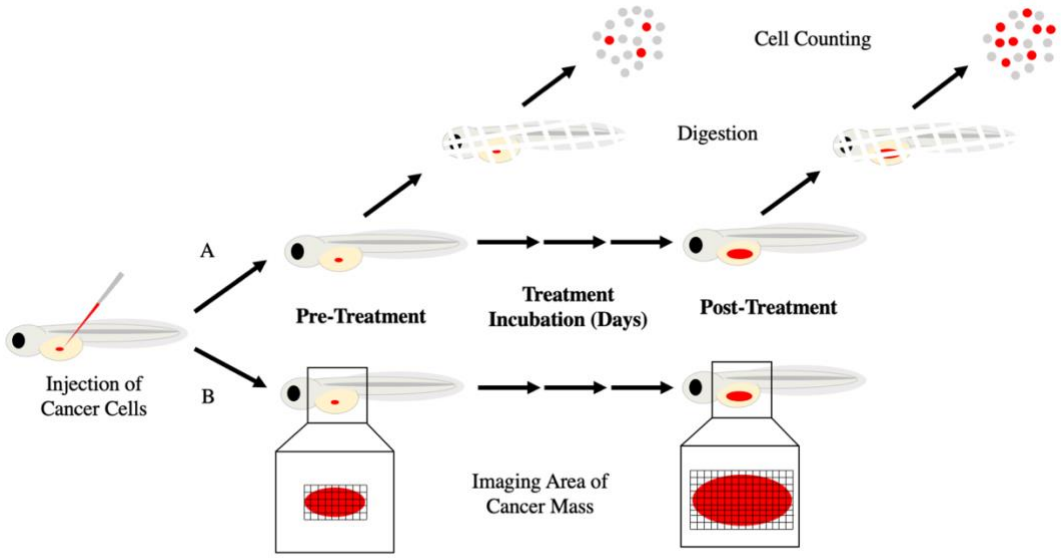

Figure 1.3. Methods of calculating cancer growth in zebrafish xenografts. Zebrafish embryos are engrafted with fluorescent cancer cells (red) by microinjection and cancer progression is accessed in one of two ways. A) Pre-treatment, a random subset of zebrafish is sacrificed, digested with collagenases and fluorescent cells are counted. The remainder of the xenografts are exposed to treatment. After treatment period, xenografts are digested, and cells are counted as before. Fold change in cell count reflects cancer growth/reduction. B) Images are taken of the fluorescent cancer cells within the zebrafish at both pre- and post-treatment with fold change in area and fluorescent intensity indicating cancer growth/reduction.

Chapter 2: Quantification of Glioblastoma Progression in Zebrafish Xenografts: Adhesion to laminin alpha 5 promotes glioblastoma microtumor formation and inhibits cell invasion

Authors: John T. Gamble, Yuriyah Reed-Harris, Carrie L. Barton, Jane La Du, Robert Tanguay, Juliet A. Greenwood

Published in the Biochemical and Biophysical Research Communications. Vol. 506, Issue 4, 2 December 2018, Pages 833-839: https://doi.org/10.1016/j.bbrc.2018.10.076

2.1. Abstract

Glioblastoma (GBM) is a deadly disease due to its ability to quickly invade and destroy brain tissue. Slowing or stopping GBM cell progression is crucial to help those inflicted with the disease. Our lab created an embryo-larval zebrafish xenograft model as a tool to study human GBM progression in an observable brain environment. The zebrafish brain is a dynamic and complex environment providing an optimal setting for studying GBM cell progression. Here we demonstrate the ability of our model to quantitate GBM proliferation, dispersal, blood vessel association, microtumor formation, and individual cell invasion by evaluating the importance of an extracellular matrix protein, laminin alpha 5 (lama5), on U251MG cell progression. Lama5 has been implicated in cancer cell survival, proliferation and invasion and is a known adhesion site for GBM cells. While lama5 is highly expressed in endothelial cells in the brain, it is unknown how lama5 affects GBM behavior. Using a lama5 morpholino, we discovered that lama5 decreased U251MG dispersal by 23% and doubles the formation of blood vessel dependent microtumors. Despite lama5 being a known attachment site for GBM, lama5 expression had no effect on U251MG association with blood vessels. Analysis of individual U251MG cells revealed lama5 significantly lowered invasion as mobile U251MG cells traveled 32.5μm less, invaded 5.0μm/hr slower and initiated invasion 60% few times per cell.

2.2. Introduction

Glioblastoma (GBM) is an aggressive brain cancer with a poor prognosis that has a median survival rate of 14 to 15 months and only 10% surviving up to 5 years [53]. Due to GBM's resistance to chemotherapy and radiation, new tumors typically develop from cancer cells that have invaded the surrounding brain tissue and escaped surgical resection [54]. GBM's invasiveness makes complete resection of the tumor impossible and results in continued growth that destroys healthy brain tissue throughout the brain, hastening death [55]. Preventing GBM invasion is integral to increasing life expectancy for those diagnosed with cancer.

Blood vessels in a brain microenvironment can have a profound impact on GBM tumor survival and ability to invade. GBM tumor cells can manipulate the blood vessels in the microenvironment by increasing vascular endothelial growth factor (VEGF) mediated angiogenesis and by invading the brain parenchyma along blood vessel basement membrane [56,57]. An important component of blood vessels are laminin proteins, a family of heterotrimeric extracellular matrix proteins that help compose basement membranes [56,58]. One alpha subunit, laminin subunit alpha 5 (lama5), is biologically active for survival, proliferation and metastasis in many cancers [59,60]. In particular, the C-terminal end of lama5 has five large globular domains (LG) that are ligands for various cellular attachment proteins capable of providing traction for migration and invasion of cancer cells [61,62]. While *in vitro* data suggest lama5 encourages aggressive cancer behavior, there is no *in vivo* evidence that lama5 contributes to the invasion of GBM along blood vessels.

Zebrafish have immerged as a cancer model due to their lack of adaptive immune system at an early age and ease of cancer cell transplantation and monitoring [18]. At the embryo and larval stages, zebrafish can be made near translucent and therefore provide an excellent visual window into a live brain environment. Within three days post fertilization (dpf), zebrafish develop a complex brain environment with extracellular matrix, glial cells, and blood flowing vessels [63]. This 3D dynamic brain structure provides an environment impossible to replicate in 2D *in vitro* systems as it provides a complex array of cells and extracellular matrix proteins. To take advantage of the zebrafish's unique characteristics, our laboratory developed

a zebrafish xenograft assay capable of effectively measuring many aspects of GBM cell progression within the brain.

Using our xenograft zebrafish model, we demonstrated GBM cell's ability to invade brain parenchyma, proliferate and associate with blood vessels [17,42]. To study how GBM/blood vessel association in a brain microenvironment affect progression, we integrated 4D individual cell tracking technology with our model that provides quantitative information of cancer cell invasion for an unprecedented examination of individual cancer cells in a dynamic *in vivo* environment. We also developed image analysis algorithms for identification of microtumors and quantification of GBM/blood vessel association. With this model, we modified the zebrafish brain microenvironment by knocking down the LG-domain of lama5 via an injection of a splice blocking morpholino, thus removing a peptide region recognized by GBM for attachment [59,64]. This design allows the direct observation of GBM cell behavior in microenvironments with and without lama5 binding sites. By transplanting fluorescently labeled U251MG cells into the mid and hindbrain ventricle of embryonic lama5 knockdown zebrafish, we gathered individual cell invasion, cancer growth, and dispersal along blood vessels throughout the brain.

2.3. Materials and Methods

Zebrafish Husbandry and Morpholino Injections

All experiments were performed with Tg(Fli1:EGFP)^{y1} zebrafish embryo-larvae (Sinnhuber Aquatic Research Laboratory) in accordance with Institutional Animal Care and Use Committee protocols at Oregon State University. Eggs were collected and staged at the one cell stage as documented in Kimmel et al., 1995 for morpholino oligomer (MO) injections. Lama5 splice-blocking MO (5′-AACGCTTAGTTGGCACCTTGTTGGC-3′) and control MO (5'-CCTCTTACCTCAGTTACAATTTATA-3') were obtained from GeneTools, LLG and diluted to 3ng/uL in ultra-pure water and 1 to 2 nL were injected into the yolk of 1-cell stage eggs. After 2 days of incubation, only embryos with specific lama5 morphant phenotype were selected from lama5 MO injected embryos, while normal developmental embryos were selected from control MO injections.

PCR and Sequencing

RNA was extracted from pools of 20 embryos at 2-day post morpholino injection. Total RNA was extracted from embryos by adding 1.3 mm zirconium beads with RNAzol® (Molecular Research Center), homogenizing embryos with a bullet blender, and following RNAzol® protocol. cDNA was created from RNA with qScript cDNA SuperMix (QuantaBio) with manufacturers protocol. Primers designed by Webb [65] were used for PCR reactions (Table S1). PCR bands of interest were cut from agarose and processed for sequencing with QIAEX II Gel Extraction Kit (Qiagen) by manufacturers protocol. Purified PCR products were sequenced by Sanger sequencing in two different reactions, one with the forward and the other with the reverse primer.

Cell Culture and Zebrafish Brain Xenografts

Human U251MG cells were obtained from the American Type Culture Collection and cultured in DMEM 10% FBS with 1% L-glu at 37°C in a 5% CO_2 humidified incubator. For labeling, U251MG cells were dyed with 2µM CM-diI (Thermo Fisher Scientific) in sterile PBS as according the manufactures protocol. Xenograft procedures were performed as previously reported [17,42]. Briefly, dyed cells were suspended in DMEM at 10^7 cells/mL and approximately 25 – 100 cells were injected into the hindbrain ventricle of 2dpf zebrafish embryos using a micro-pressure injector.

Microscopy

For all imaging, zebrafish larvae were anesthetized in 0.2mg/mL MS-222 E3 medium (EM) + phenylthiourea (PTU) solution and immobilized on glass slide bottom dish or glass bottom 96 well plate, dorsal side down, in 0.8% low melting point agarose with 0.2mg/mL MS-222 EM + PTU. For time-lapse imaging, 100uL of 0.2mg/mL MS-222 EM + PTU solution was added on top of agarose to prevent it from drying out and larvae were maintained at 33°C. All imaging was done on a Zeiss 780 LSM confocal microscope (Carl Zeiss Microscopy) with 20x objective lens. To access U251MG growth, xenograft larvae were imaged at 1 and 4 day post-injections (dpi) with overlapping 4µm z-slice sections so all fluorescently visible cells were captured in 3D. For time-lapse images, the top 160 to 200µm of the cranium

was imaged every 10 mins. Using these parameters, we were able to image each zebrafish in 1.25 - 2.5 mins, allowing us to image 4 to 8 xenografts at one time.

Image and Data Analysis

Image analysis was performed using ImageJ/Fiji software (NIH) [66]. To determine U251MG progression, all images were processed with 3D median filtering where GBM cells were thresholded with Otsu algorithm and blood vessels with Triangle algorithm [67–69]. Cell counting was conducted using 3D Object Counter (ImageJ/Fiji-based object identification tool) [70]. Objects with a radius larger than 15µm were split into multiple cells according to that radius. Dispersal was calculated by determining the centroid from all the cell positions detected and the distance of each cell to the computed centroid was averaged together. Microtumors were classified having a radius equal to or larger than 25µm and having a depth of 60µm or greater from the dorsal side of the cranium to eliminate the location of the transplantation site.

For counting U251MG blood vessel associations, binary thresholds from U251MG cells and GFP expressing blood vessels images were used to create an image where only overlapping pixels with the same coordinates were used to create a new blood vessel association image. 3D Object Counter acquired 3D location, volume, and number of U251MG cell blood vessel associations for each larva.

For time-lapse images, Correct 3D Drift (ImageJ/Fiji-based registration tool) was used to minimize movement of cells due to larvae growth [71]. To obtain 3D coordinates for cells across all time points, Trackmate (ImageJ/Fiji-based tracking tool) was used via the "Linear Motion LAP Tracker" algorithm. To rule out the possibility of cells being tracked multiple times, only cell tracks with time frames greater than half the length of the time-lapse experiment were used for analysis. For invasion analysis, a cell was considered to be invading if its velocity exceeded 0.5µm/min. For invasion initiation, cells were counted for the number of times in which their velocity went from below 0.5µm/min to above 0.5µm/min.

All statistics were generated by JMP® Pro 13 (SAS) where comparisons between control and lama5 morphant used Student's T Test and comparisons between time-points for microtumors used Fisher's exact test.

2.4. Results

2.4.1 *Zebrafish Xenograft Model*

In previous studies, we validated the zebrafish xenografts model's ability to accurately and consistently provide GBM proliferation and invasion data [17,42]. To learn more about GBM cell invasion in a brain environment, we integrated confocal microscopy to gather detailed 3D images to follow individual GBM cell invasion and distinguish cells interactions with blood vessels. Using this model, fluorescently dyed U251MG cells could be identified up to a depth of 250um within the zebrafish brain. Images and subsequent analysis of larval brains taken at 1 and 4dpi provided GBM cell volume and 3D coordinates inside each larvae brain. Analysis of control xenografts displayed increases in log2 fold change of 0.54 and 0.59 for cell number and dispersal, respectively, similar to previous studies [17,42] (Figure S1A,B). Upon examination of U251MG density patterns in the brain, we detected microtumors, or cell masses with blood vasculature. Masses with radii larger than 25μm were identified as microtumors (Figure 2.1.A). Surprisingly, one day after transplantation, microtumors formed in several of the control larvae and by 4dpi the number increased significantly with some larvae having up to 3 microtumors.

When Tg(Fli1:EGFP)^{y1} zebrafish were used, vascular information could be collected to provide data on GBM cell associations with the blood vessels. Data revealed GBM cell/blood vessel associations occurring by 1dpi with the majority of larvae having associations by 4dpi. To investigate tumor growth by blood vessel association, 3D coordinate data obtained for blood vessel association sites were identified as being associated with a microtumor or individual U251MG cell based on there the proximity to determined microtumors. Analysis revealed all identified microtumors had blood vessel associations, strengthening the argument they are behaving as tumors (Figure 2.1.B).

In order to analyze individual GBM cell invasion within a brain environment, time-lapse microscopy was implemented. Visual analysis of 3D time-lapse data showed dynamic movement of many U251MG cells in control larvae (Figure 2.1.C-E). Some U251MG cells quickly navigated through the brain by long cellular

protrusions seen in mesenchymal-type invasion [33]. Interestingly, U251MG cells could be seen associating and migrating along blood vessels where in one instance, a single U251MG cell attached and physically pulled blood vessels into different locations (Figure 2.1.D). With this data, it was possible to classify the invasive and non-invasive cells as well as individual cell statistics (Figure 2.1.E). U251MG cell invasion was analyzed by measurable statistics such as distance traveled, velocity and invasion rate (number of times a cell's velocity exceeds 0.5μm/min per hour).

2.4.2 *Laminin Alpha 5 Zebrafish Knockdown*

Our new zebrafish xenograft model was used to determine lama5's impact on GBM progression. To do so, we knocked down the expression of full-length lama5 using an antisense MO. The MO recapitulates the *m538* mutation found in zebrafish that results in partial loss-of-function due to truncation of the LG domains, known substrates for cellular adhesion [65]. Knockdown of lama5 resulted in the expected phenotype, causing truncation of the yolk sac tail extension and tail fin dysmorphogenesis (Figure 2.2.A) [65]. A negative control standard control MO that targets a human beta-globin intron mutation, produced no observable phenotype. Forty percent of lama5 morphants displayed irregular blood vessel formation at the dorsal midline junction in the brain (Figure 2.2.B). Despite disorganization, blood cells were flowing through enclosed blood vessels as observed under a bright-field microscope. Using lama5 primers spanning the MO target site, mRNA extracted from 2dpf lama5 morphants displayed an inclusion of approximately 200bp of intronic RNA (Figure 2.2.C) [8]. Sequencing of PCR products confirmed that the intron inclusion resulted in a premature stop codon, which closely mirrors the *m538* allele (Figure 2.2.D and Figure S2) [65].

2.4.3. *Laminin Alpha 5 Decreases U251MG Dispersal and Increases Microtumors*

Lama5 has been implicated in increasing proliferation and mobility of cancer cells [64,72]. To assess lama5 effects on GBM progression, U251MG cells were fluorescently dyed and transplanted into the brain of lama5 morphants and control Tg(Fli1:EGFP)^{y1} zebrafish embryos at 2dpf (Figure 2.3.A). Experiments resulted in 74 control and 57 lama5 morphants with 92% and 77% survival in control and lama5 morphants, respectively (Figure S3). U251MG dispersal data revealed similar

dispersal throughout the brain between lama5 morphants and control larvae at 1dpi. However, by 4dpi the average log2 fold change for dispersal was 23% higher for lama5 morphants (Figure 2.3.B). U251MG cell counts were nearly identical (Figure 2.3.C). In total, 55 microtumors were identified within both control and lama5 larvae, with controls having a higher percentage of larvae with microtumors at both 1 and 4dpi time points. Control larvae were found to be twice as likely to develop the formations with 32% of controls displaying microtumors compared to 16% of lama5 larvae (Figure 2.3.D). To assess GBM/blood vessel associations, we verified blood vessel density was not affected by lama5 knockdown by calculating blood vessel volume from images. No differences were seen between groups (Figure 2.3.E). Data revealed a similar number of associations per larva as well as percentage of larva with associations for both control and lama5 morphants at 1 and 4dpi (Figure 2.3.F-G).

2.4.4. *Microenvironmental Laminin Alpha 5 Slows Glioblastoma Cell Invasion In Vivo*

To assess lama5's effects on GBM mobility, fluorescently dyed U251MG cells were transplanted into the brain of lama5 morphant and control zebrafish larvae at 3dpf. Nine lama5 morphant larvae and eight control larvae were analyzed for U251MG cell movement over the course of five experiments as one control larva died during imaging. Thus, 331 and 500 total cells from lama5 morphant and control larvae respectively had their position tracked over time while within zebrafish larvae brains (Figure 2.4.A). A significant difference was found in cell activity for lama5 morphant larvae as 71% of U251MG cells traveled more than 100μm, compared to 51% in control larvae, confirming dispersal data. Histogram data showed a positive shift for lama5 morphants indicating increased cell mobility (Figure 2.4.B).

U251MG cells were categorized as non-invasive if they invaded less than 5% of the tracking duration. Lama5 morphant larvae had a significantly lower percentage of non-invasive cells than controls, 21.7% to 35.5% respectively (Figure 2.4.C). To quantitate specific invasive behaviors impacted by lama5, all non-invasive cells were removed from further analysis to prevent skewing results. U251MG cells in lama5 morphant larvae traveled 32.5μm farther and 5.0μm/hr faster than in control larvae (Figure 2.4.D,E). A 20% and 60% increase in U251MG invasions per hour and cell,

respectively, was seen in lama5 morphants, indicating that lama5 may be inhibiting the invasion process (Figure 2.4.F,G).

2.5. Discussion

Despite advances in cancer therapeutics and treatment, GBM treatment has lagged behind as current therapies fail eliminate GBM progression [53,54]. Presently, there is limited information on how the brain microenvironment influences GBM invasion and tumor formation. Considering lama5 helps to compose the basement membrane of blood vessels and GBM cells associate with vasculature in the brain, we utilized our zebrafish xenograft *in vivo* model to study how lama5 affects GBM progression [58]. Surprisingly, our results indicate that lama5 discourages U251MG dispersal and decreases invasion despite evidence indicating lama5 as pro-migratory in *in vitro* settings [60]. Interestingly, anti-VEGF therapies cause a similar increase in GBM invasion as cells become resistant to therapy and mesenchymal activity increases despite continued ablation of VEGF activity [73]. PTEN deficient GBM tumor cells, such as U251MG, express elevated VEGFR2 [74]. In one study, VEGFR2 knockout induced highly invasive behavior in mouse xenografts indicating GBM VEGF activity negatively correlates with invasion [75]. In addition, lama5 attachment has been shown to promote VEGF activity in some cancer cell lines [76]. Therefore, lama5 attachment may increase GBM VEGF activity, subsequently reducing invasion. We also report that lama5's presence promotes microtumor formation with U251MG cells. Microtumors were seen having blood vessels in and around formations suggesting VEGF induced angiogenesis. We hypothesize that GBM cell adhesion to lama5 may be decreasing cell invasion by elevating GBM VEGF activity which suppresses invasion mechanisms and results in increased tumor formation. More studies are needed to verify specific connections between lama5 adhesion and VEGF activity.

Zebrafish xenograft cancer models provide advantages over mouse models as they provide a translucent and compact environment comprising a complex array of extracellular components. Furthermore, transgenic zebrafish lines such as the Tg(Fli1:EGFP)^{y1} offer the ability to view cancer cell interactions with intact blood

vessels. In order to better understand GBM progression, we developed a novel *in vivo* method for quantifying cancer progression in 4D. Here we demonstrated our model's ability to measure proliferation, dispersal, microtumor formation, blood vessel association and invasion rate, and provided assessable attributes to compare and help elucidate mechanisms of progression. This is a significant advancement to *in vivo* models as this model provides insight into how cancer cells, already displaced from the primary tumor, invade through tissue and establish new tumors. This is especially important for studying GBM as this is the primary reason for patients succumbing to the disease. Additionally, our model is amenable for GBM drug discovery, as zebrafish's compact size and quick developmental time offer capably for higher replicated numbers and high-throughput screening potential [24,42]. With growing emphasis on preventing GBM spread, this model provides a large set of measurables to assess potential therapeutic effectiveness and mechanism of action.

Acknowledgements

We would like to thank Annie-Marie Girard-Pohjanpelto from the Center for Genome Research and Biocomputing at Oregon State University for her help in confocal training and imaging advice. We are grateful to the Sinnhuber Aquatic Research Laboratory for providing access to molecular biology equipment, supplies and zebrafish husbandry. Our work was supported in part by NSF grant 1310657 and NIH grant P30 ES000210.

2.6. Figures

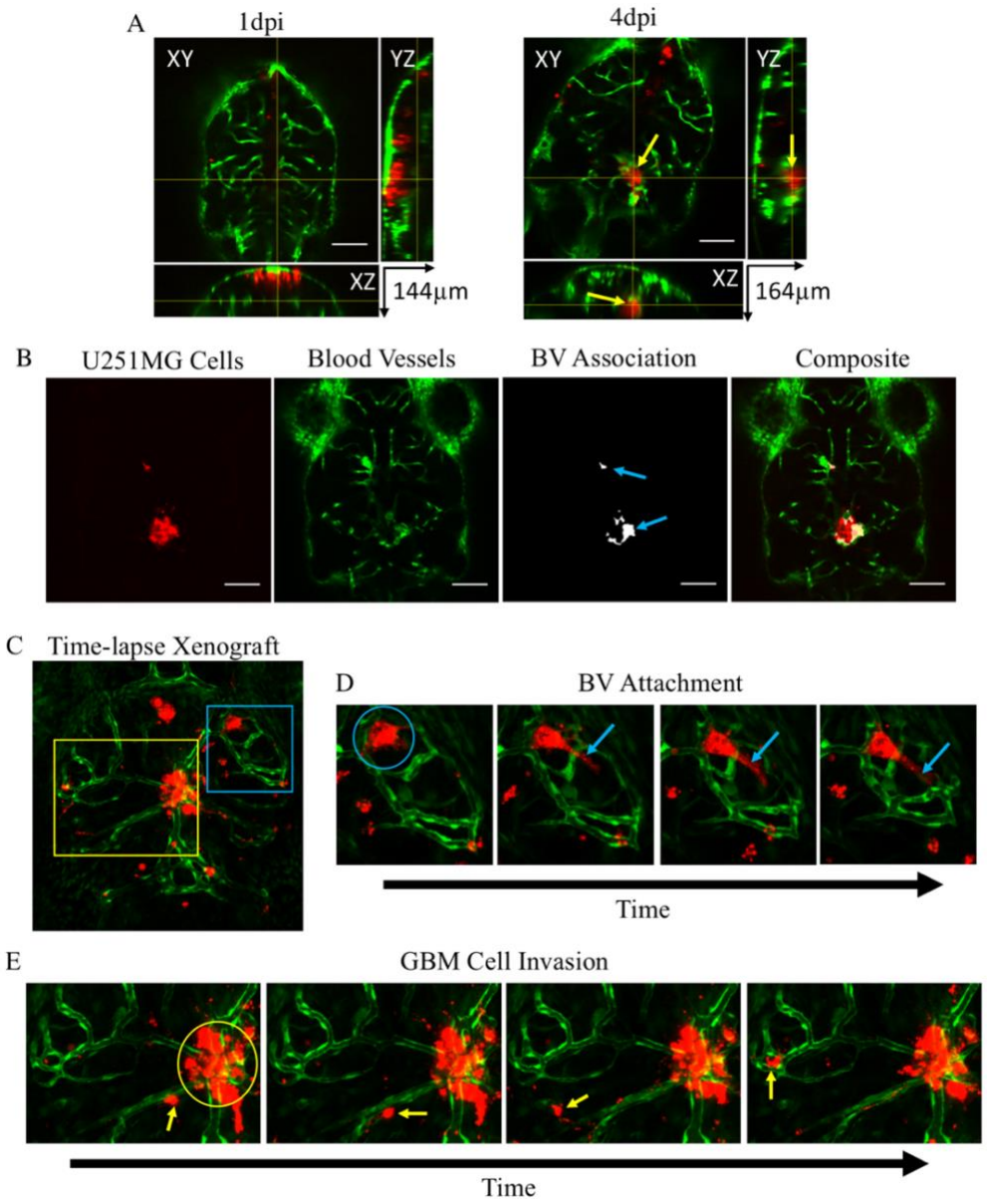

Figure 2.1. Zebrafish Brain Xenograft. A) Orthogonal views for Z-section of zebrafish brain with U251MG cells (red) and blood vessels (green) at 1 (Left) and 4 (Right) day post injection displaying microtumor formation (yellow arrow) occurring deep in brain surrounded with blood vessels. B) Representative panels of calculating U251MG cells associations with blood vessels (BV). 100µm scale bar. C) Maximum projection image frame of 3D time-lapse image of zebrafish brain with blood vessels (green) and transplanted U251MG cells (red) with areas of interest indicated. Blue box: BV attachment. Yellow box: GBM cell invasion. D) Representative time-lapse

images of U251MG cell attaching to blood vessels (blue circle) and constricting with pseudopodium (blue arrows). E) Representative time-lapse images of U251MG cell invading zebrafish brain (yellow arrows) and non-invasive U251MG cells (yellow circle).

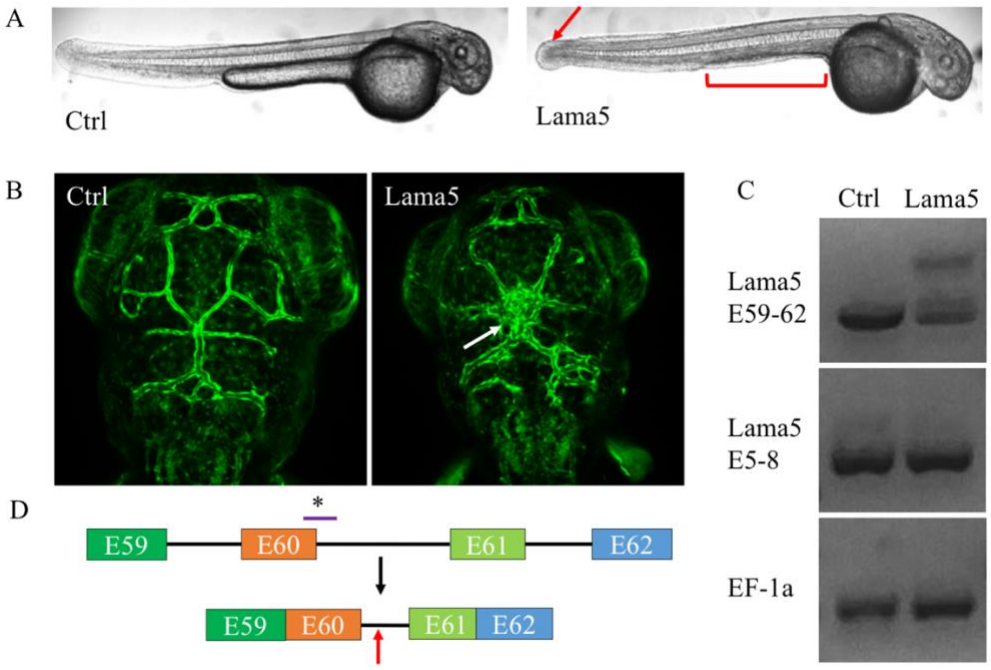

Figure 2.2. Lama5 morpholino causes creates cryptic intronic splice resulting in m538 phenotype. A) Zebrafish embryos at 2 days post fertilization (dpf) after control (left) or lama5 (right) MO injection. Red arrow indicates reduced tail fin growth. Red bracket indicates loss in yolk sac extension. B) Maximum projection images of blood vessels in the brain of zebrafish larvae at 2 days after control or lama5 MO injection. White arrow indicates disorganized dorsal midline junction of cranial blood vessels. C) Agarose gel of cDNA made from mRNA extraction of pooled zebrafish embryos (20) 2dpf after control or lama5 morpholino (MO) injection. Lama5 E59-62 comprises laminin alpha 5 exons 59 to 62 while lama5 E5-8 comprises exons 5 to 8. D) Lama5 MO causes cryptic intronic splice of lama5 mRNA that includes a fragment of intron 60-61. *Location of MO binding. Red arrow indicates introduction of premature stop codon.

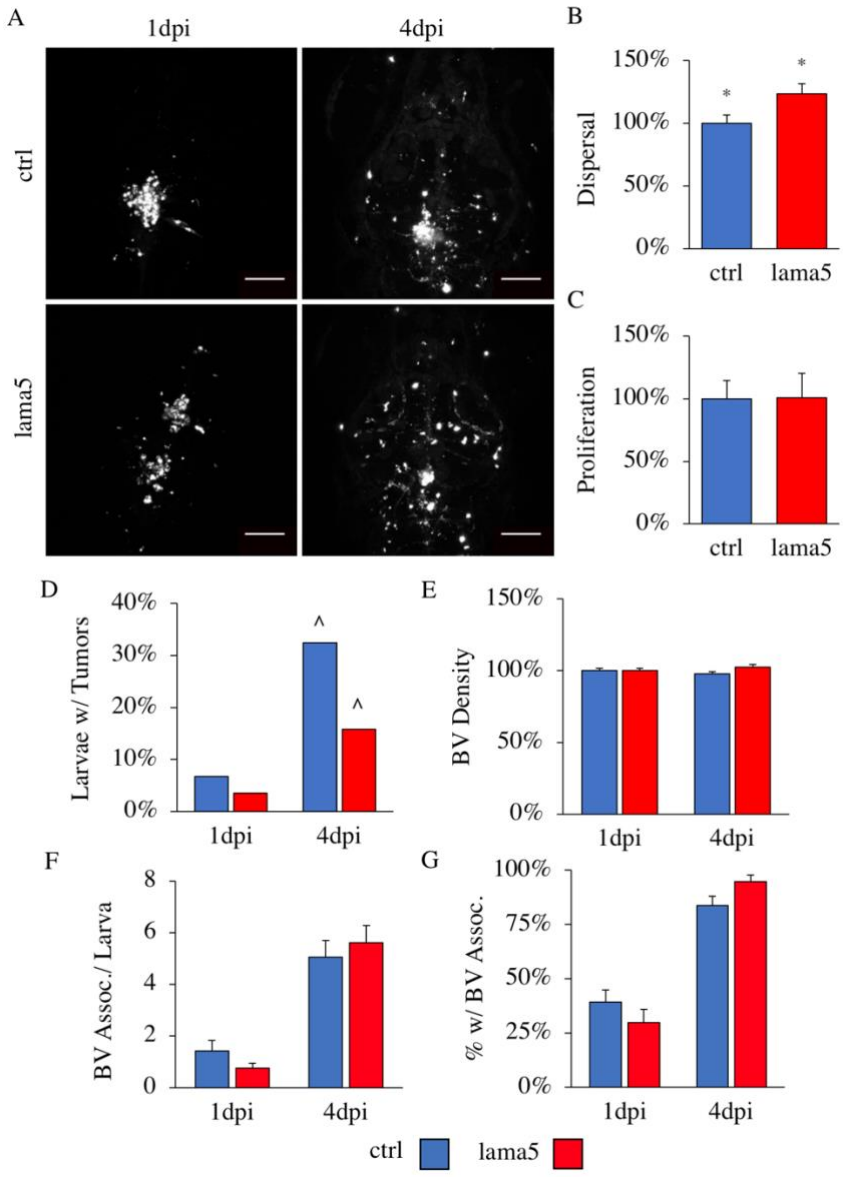

Figure 2.3. Laminin alpha 5 increases U251MG microtumor growth but not blood vessel association. A) Representation of U251MG dispersal for lama5 KD and control larvae at 1 and 4dpi; 100µm scale bar. B-C) Percent dispersal and proliferation as compared to control for U251MG cells. D) Percent larvae with microtumors. E) Percent blood vessel (BV) density as compared to control at 1 and 4dpi. F) Average U251MG/BV associations per larva. G) Percent larvae with U251MG/blood vessel associations. Lama5 n=57, control n=74; *$P < 0.05$, Student's T Test; SEM bars shown; ^$P < 0.05$, Fishers Exact Test.

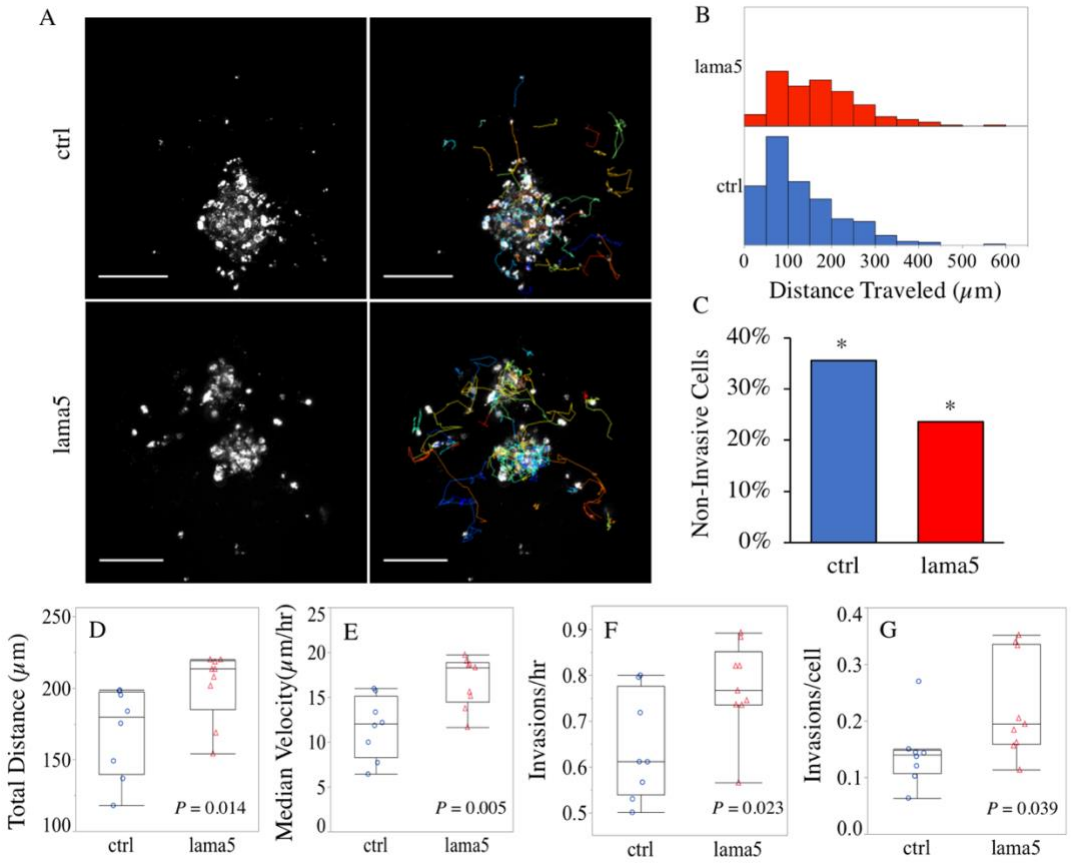

Figure 2.4. Laminin alpha 5 inhibits invasion in a brain microenvironment. A) Representative maximum projection images of 4D U251MG cell tracking in zebrafish larvae brain. Left to right: CM-DiI-labeled U251MG cells and Trackmate calculated tracks where each color represents the 4D coordinate data of individual cells; 100μm scale bar. B) Histogram of distance traveled for all U251MG cells (lama5 n=331, control n=500). C) Percentage of non-invasive U251MG cells for control and lama5 KD larvae. *Fisher's Exact Test, $P < 0.001$. D-G) Average total distance (D), average median invasion rate (E), average number of times invasion was initiated per hour (F), average number of times invasion was initiated per cell (G), for lama5 (n=9) and control (n=8) zebrafish where each point represents the average U251MG cell statistic per larva. P-values determined by Student's T Test.

Chapter 3: 4D Quantitative Image Analysis of Cancer Cell Invasion in a Brain Microenvironment Using ImageJ Software

Authors: John Gamble, Robert Tanguay, Juliet A. Greenwood

Microsc. Microanal. 23 (Suppl 1), 2017

doi:10.1017/S1431927617006572

3.1. Article

Acquisition of quantitative data of individual tumor cell invasion within live brain environment is currently limited. Individual cell monitoring is needed to understand cellular mechanisms for aggressive cancer behavior so that these mechanisms can be targeted or exploited for therapies. While numerous in vitro systems are well adapted to elucidate these mechanisms, they lack a dynamic environment that present numerous cell signals, mechanical forces and host cell interactions that combine to provide complex conditions that influence cell behavior. It is this complex microenvironment that cancer is found in humans and therefore it provides the optimal conditions for studying tumor cell invasion. Zebrafish have gained traction as a vertebrate animal model for cancer studies where at three days of age, larvae have functional vasculature and compartmentalization of the brain that can provide transplanted human brain tumor cells a microenvironment that recapitulates brain conditions. With their translucent and small confided brain, tumor cells can be monitored via fluorescent microscopy in extreme detail with visual access to the entire brain. To study glioblastoma (GBM), a very aggressive and deadly brain cancer, our lab has developed an in vivo model where fluorescently dyed human cancer cells are transplanted into the brain of larval zebrafish to monitor progression of the tumor cells (Figure 3.1.A) [17]. This model led to discoveries in GBM invasion and potential treatments to slow that invasion were made [17,42]. While these discoveries were impactful, they did not provide data for individual invasion mechanisms of tumor cells that were affected by treatments or knockdown of protein expression. To fill this gap, we integrated cell tracking through time-lapse confocal imaging into the model so that transplanted GBM cells within the zebrafish brain microenvironment could be monitored differences in invasive behavior. To accomplish this, larvae with GBM cell transplants were anaesthetized, embedded in low melting point agarose on a glass slide bottom petri dish and covered in anaesthetizing media allowing larvae to survive up to 18hrs. Depending on imaging speed of the microscope, z-stack images of the fluorescent cancer cells within zebrafish brain could be taken every 1 to 10min for up to eight larvae. Detailed 4D

images of the entire tumor cell population in the brain microenvironment were produced.

Using ImageJ software (Fiji), 4D images of the population of individual tumor cells in larva brains can be automatically tracked to provide a litany of quantifiable data [66]. After performing drift correction using the "3D Drift Correction" plugin to remove any movement not attributed to the tumor cells, the Trackmate plugin can be used to methodically detect and track the tumor cells as they move throughout the brain [71,77]. Trackmate uses consecutive modules that identify objects in 3D, creates linkages between the same object from time-point to time-point and then compiles object tracks that represent, in this case, cells movement throughout the brain over time (Figure 3.1.B, C, D). Numerous settings are available for all modules that are customizable for differences in cell phenotypes and as well as fluorophores used for tagging cells. Quality of tracking can be assessed visually throughout the process to make ensure proper identification of cells and their movements. Trackmate will generate useful data for each cell such as mean velocity and displacement, but raw 4D position data of individual cells can be exported for other analyses. The resulting data contains information on the invasiveness of individual tumor cells in brain tissue. Typically, tumor cell invasion data only provides information on whether a cell is capable of invasion. Data from this method can generate many different quantifiable tumor cell invasion statistics that can help in elucidating specific mechanisms used by cells to maneuver or invade through a brain microenvironment (Table 1). These statistics can be used to help determine in what ways invasion is affected for tumor cells exposed to potential therapies or alterations in protein expression. Parameters for invasiveness can be set to create subpopulations of tumor cells where the subpopulations are seen to have different responses. All this leading to reliable data that can be more easily compared across studies.

3.2. Table

Cell Statistic	Description	Interpretation
Mean Velocity	Average velocity of cell throughout imaging	Describing invasive efficiency based on speed.
Min Velocity	Minimum velocity of cell between time points	Can be used as parameter for non-invasive cells.
Max Velocity	Maximum velocity of cell between time points	Reveals if invasion potential is affected once invasion is initiated.
Total Distance	Total distance traveled by cell	Can be used as parameter of non-invasive cells.
Displacement	Distance from origin to end position of cell	Can be used as parameter of non-invasive cells.
Directionality	Cell efficiency of traveling from origin to end position	Describes invasive efficiency based on distance.
Invasiveness	Percent time spent invading	Describes aggressiveness of cell.
Invasion Rate	Number of times a cell initiates invasion for a length of time	Describes the cells propensity to invade.
Invasion Initiation Rate	Average time needed to initiate invasion	Describes quickness of cell to initiate invasion.

Table 3.1. Summary of quantitative data that can be collected from individual invasive tumor cells using model.

3.3. Figure

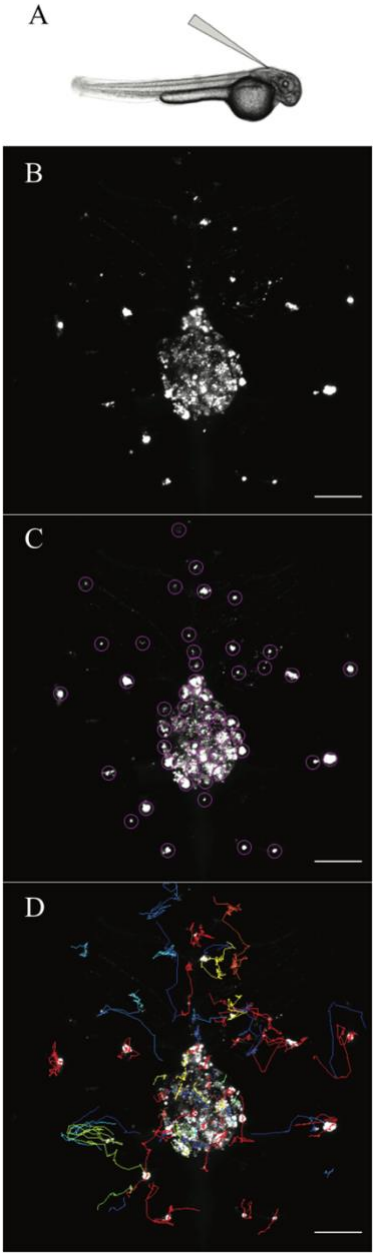

Figure 3.1. Glioblastoma cell invasion tracking in zebrafish xenograft. (A) Glioblastoma (GBM) cell transplant site for 3 days post fertilization larva. (B) 2D representation of 3D images of GBM cells invading zebrafish brain. (C) Detection of GBM cells with ImageJ Trackmate plugin are shown with circles. (D) Individual GBM cell tracks shown provide quantitative invasion data for each cell. 50µm scale bars on bottom right of each image.

Chapter 4: Using an embryo-larva zebrafish xenograft assay in the discovery of new Bcl-2 functional converter drugs

Authors: John T. Gamble, Martin C. Pearce, Erin Morgan, Robert Tanguay, Norbert Reich, Juliet A. Greenwood, Siva Kumar Kolluri

Data Included in Section 4.3.2 is sourced from:
Oncotarget. 9 (40), 2018

doi:10.18632/oncotarget.25437

4.1. Abstract

The anti-apoptotic ability of Bcl-2 has become a hurtle in the treatment of many cancers. Overexpression or increased activity of Bcl-2 and other anti-apoptotic proteins can overcome treatment of chemotherapy, emboldening aggressive cancers. Interestingly, Bcl-2 can be converted into a pro-apoptotic protein that can inhibit other anti-apoptotic proteins. To study multiple potential Bcl-2 functional converting drugs, we employed an embryo-larva zebrafish xenograft model. This model provides a simple *in vivo* environment for human cancer cells to habitat where cancer progression can be easily assessed when testing drugs early in development. A peptide capable of converting Bcl-2, NuBCP-9, was able to effectively reduce cell viability and induce apoptosis in chemoresistant lung cancer. Using antibodies for Bcl-2's pro-apoptotic form, Bcl-2 functional conversion was confirmed with peptide treatment in the resistant cancer line. Additionally, when transplanted into zebrafish embryos, the chemoresistant cancer mass was significantly decreased when compared to vehicle. To aid in delivery of NuBCP-9, a nanoparticle light-delivery method was developed. Using hollow gold nanoparticles, we delivered NuBCP-9 into cells and successfully released the peptide from endosomal entrapment by near-infrared laser exposure. Furthermore, delivery was tested *in vivo* as zebrafish xenografts with nanoparticle-NuBCP-9 treated chemoresistant cells displayed significantly lower cell growth after near-infrared light exposure compared to no light exposure. Lastly, multiple small molecule Bcl-2 functional converting drugs were tested in cell-based and in zebrafish xenograft assays. Results identified two compounds capable of reducing cell viability and *in vivo* cancer growth for chemoresistant lung cancer and a triple negative breast cancer line as well as not causing toxic effects to zebrafish embryo-larva.

4.2. Introduction

The B-cell lymphoma 2 (Bcl-2) family comprises both pro- and anti-apoptotic proteins that work in concert to either maintain cell survival or initiate cell death. Bcl-2 is an anti-apoptotic protein that serves an integral part in preventing apoptosis, initiated by permeabilization of the mitochondrial membrane [78,79]. Bcl-2 is now considered an oncogene as many cancers, including lung and triple negative breast cancers, overcome programmed cell death by increasing Bcl-2 expression [80,81]. Bcl-2 is one of many proteins in the Bcl-2 family that regulate cell apoptosis via Bcl-2 homology (BH) domains. The BH3 domain is of special interest as it incorporated in all pro-apoptosis proteins, earning the label "death domain" [79]. Interestingly, despite Bcl-2 having anti-apoptotic activity, it contains a BH3 domain. Researchers have discovered that a nuclear receptor protein, Nur77, is capable of binding Bcl-2's loop domain and exposing its BH3 domain [82,83]. In the nucleus, Nur77 can assist in cell proliferation, however, in the cytosol it associates with the mitochondria and can induce apoptosis [84,85]. Nur77 induced conversion of Bcl-2 allows it to activate pro-apoptotic proteins as well as inhibit other anti-apoptotic proteins, effectively turning Bcl-2 into a death protein. As a result, researchers have searched for the means to activate this ability with Bcl-2 function converters (BFCs) in hopes of activating apoptosis in overexpressing Bcl-2 cancers.

Peptides have the potential to be highly specific, bind with high affinity and have low toxicity [86]. Just as proteins can inhibit or active specific proteins, peptides derived from those protein sequences have been found to do the same. Interestingly, peptides derived from the Nur77 peptide sequence are capable of converting Bcl-2 into a pro-death protein [87]. With the addition of a cell penetrating D-arginine octamer, a 9-amino acid Nur77 peptide, NuBCP-9, is capable of entering the cell and selectively induce apoptosis in cancer cells with high Bcl-2 levels. While peptide BFCs are promising, peptide drugs suffer from poor bioavailability as peptides can be easily cleaved by proteolytic enzymes and can become trapped in cellular endosomes. [86,88]. Nanoparticle technology has offered the ability to increase drug half-life and reduce needed treatment concentration as they can protect against degradation and increase treatment availability. Hollow gold nanoparticles (HGNs) may provide a

solution to the peptide delivery problem. HGNs are biologically inert and can be orthogonally loaded with various items including peptides through thiol-gold bonds. Additionally, HGN's possess the ability to convert near-infrared (NIR) light energy into thermal energy, releasing cargo [89,90]. This light releasing capability could allow for location specific delivery of peptide therapeutics within a patient as well as provide a mechanism to escape endosomal encapsulation and target cytosolic Bcl-2.

While peptides suffer from poor pharmacodynamics but have low toxicity, small molecules drugs provide better bioavailability, but increased risk of toxicity due to less specificity. Some small molecule Bcl-2 inhibitors have already been proven successful, such as ABT-199 (Venetoclax®), which has been approved for treatment of chronic lymphocytic leukemia [91,92]. These Bcl-2 inhibitors work by disrupting Bcl-2's anti-apoptotic function, allowing pro-apoptotic proteins to commit to cell death. Unfortunately, these inhibitors can result in resistant cancers as tumor cells adapt by increasing expression of other anti-apoptotic proteins, like Bcl-xL [87,93]. Ideally, a small molecule drug would be capable of binding Bcl-2 and converting it into a pro-apoptotic protein, much like NuBCP-9, and inhibiting anti-apoptotic proteins like Bcl-xL. This ability to convert an apoptosis inhibitory protein into a promoting protein limits the cell's capacity to gain resistance, resulting in a more effective drug.

To aid in BFC testing, we applied an embryo-larva zebrafish xenograft assay. *In vitro* data is not a good predictor for drug success. Cell cultures lack important environmental complexities that greatly influence cancer cell reactions to drugs where the environment can either physically impact drug delivery or biochemically effect cancer response to the drug. It is therefore important to conduct *in vivo* testing to efficiently discover therapeutics that will have impact [63,94]. Zebrafish models offer an approachable *in vivo* model that can provide significant results to researchers early in drug discovery. At embryonic-larval stages, zebrafish can be housed in multi-well formats and can be treated by immersion into minimal volume, conserving limited experimental treatments. Additionally, at these young ages, zebrafish have developed organ systems, i.e. heart, liver, brain, and are capable of providing valuable toxicology information as they are sensitive to small molecule compounds during

development [36]. At embryonic-larval stages, zebrafish lack an adaptive immune system and therefore do not require immune suppression for human cancer cell transplants [95]. Despite their small size, zebrafish have a large yolk sac capable of containing hundreds of cancer cells, offering ample space to transplant a significant number of cells for drug testing [16,96,97]. Moreover, zebrafish are also amenable to optical microscopic imaging. At these stages the fish are nearly translucent and allow for an excellent view of the entire organism. This developmental advantage provides researchers the ability to capture cancer progression non-invasively allowing multiple measurements within the same organism, increasing confidence in statistical measurements. By fluorescently dyeing and transplanting multiple different human cancer cell lines into zebrafish embryos, we were able to track cancer growth and survival as they were exposed to various potential cancer therapeutic drugs.

4.3. Results

4.3.1. *Zebrafish Xenograft Assay*

To effectively test potential cancer drugs *in vivo*, we implemented a zebrafish xenograft assay. For the assay, human cancer cells were fluorescently dyed with CM-diI cell tracker dye and transplanted via injection into the yolk sac of 2 days post fertilization (dpf) zebrafish embryos (Figure 4.1A). Transplanted cells were allowed to establish themselves overnight and were then imaged to assess cancer cell mass. Xenografts were maintained in embryo-larva media for 3 days until they were imaged again for a final assessment of the cancer cells. To measure cancer cell growth and survival, ImageJ/Fiji (NIH) software was used [66]. Raw multi-Z plane images were processed to produce a maximum intensity projected and median filtered image and both cell area and average fluorescent intensity were calculated to provide intensity density, mean intensity * area, using the Otsu algorithm. (Figure 4.1B) [68]. Intensity density therefore provided information on both the size and density of cells within the yolk as higher intensities were correlated with an increased number of cells per area. Average log2 fold changes in intensity density for xenografts from 1 to 4-day post injection (dpi) between groups indicates treatment effectiveness *in vivo*.

4.3.2. *Chemoresistant Lung Cancer Susceptible to Bcl-2 Functional Converting Peptide*

Overexpression of Bcl-2 is a known pathway for cancer cell avoidance of apoptosis. Notably, increased expression of Bcl-2 in cancer can gain resistance to chemotherapies, resulting in difficult to treat cancers [80,81]. Our lab produced a multi-chemotherapy resistant cell line by exposing H460 lung cancer cells to paclitaxel in low doses until resistance was gained. Paclitaxel resistant (PacR) H460 cells had increased cell viability and decreased percentage of apoptotic cells when exposed to paclitaxel compared to parental H460 cells (Figure 4.2A,B). Resistance to paclitaxel also resulted in resistance to another chemotherapy, doxorubicin, despite no previous exposures (Figure 4.2A). Bcl-2 expression was found to be increased in this resistant line compared to the parental (Figure 4.2.C). Additionally, Bcl-2 expression was negatively correlated with cleaved caspase 3 presence when exposed to paclitaxel indicating prevention of apoptosis (Figure S4). Coupled with a cell internalizing arginine tag, NuBCP-9, a 9 amino acid peptide sequence derived from Nur77 protein, is capable of transforming Bcl-2 from a pro-survival to a pro-death protein [87]. NuBCP-9 exposure resulted in loss in cell viability for both PacR and parental H460, but significantly induced apoptosis in more PacR H460 cells (Figure 4.2D,E). Exposure to NuBCP-9/AA mutant had no effect on cell viability. Furthermore, flow cytometry using BH3 domain fluorescently tagged antibodies, revealed BH3 domain exposure in both parental and PacR cells 24hrs post NuBCP-9 indicating transformation of Bcl-2 into a pro-death protein confirmation (Figure 4.2F). No conformational changes were seen with a Bcl-2 conformation independent antibody when NuBCP-9 was introduced (Figure S5).

While NuBCP-9 is capable of reducing cancer cell viability *in vitro*, there is little evidence that it can cause cell death *in vivo*. To determine this, we applied our zebrafish xenograft assay. PacR H460 cells were dyed with a fluorescent dye and exposed to NuBCP-9 for 6hrs before being injected into the yolk sac of embryonic zebrafish. Due to poor absorption and peptide degradation, pre-treatment of NuBCP-9 was necessary to ensure exposure to the peptide. NuBCP-9 exposed cells incubated in zebrafish xenografts for 3 days were imaged by confocal microscopy at 1 and 4 dpi.

Image comparisons between xenografts, display smaller PacR H460 masses for NuBCP-9 exposed cells than for controls (Figure 4.2G). Analysis of xenograft image data confirms that there is a significant decrease in NuBCP-9 exposed PacR H460 cells compared to controls and thus suggests that NuBCP-9 is capable of killing cancer cells *in vivo* (Figure 4.2H).

4.3.3. *Hollow Gold Nanoshell Delivery of NuBCP-9*

While the use of peptides for cancer treatment shows promise, there are many challenges that must be overcome. While cell penetrating peptides, such as NuBCP-9, can effectively enter the cell, large concentrations are required for the desired response due to endosomal entrapment [98]. In an effort to overcome this problem, hollow gold nanoparticle (HGN) technology was used to aid in NuBCP-9 delivery. Assembly of HGN-NuBCP-9 nanoparticles were constructed by addition of single stranded thiol-DNA amines to the HGN surface. Subsequent addition of complementary DNA strands allowed for particle tracking, FAM-tagged DNA, and internalization via a DNA-biotin tag. Further addition of streptavidin and a biotinylated cell penetrating peptide, TAT (Biotin-YGRKKRRQRRRPQ), allowed for the nanoparticle to enter the cell. Functionalization of the terminal amine on the thiol-DNA strand with nitrilotriacetic acid (NTA) allowed for addition of His-tagged NuBCP-9 peptide to the HGN (Figure 4.3A).

Upon entry into a cell, irradiation with an 800nm NIR light will cause HGN nanoparticles to release their cargo (Figure 4.3.B) [89,90]. NuBCP-9 release will result in cell apoptosis if Bcl-2 levels are elevated enough. To verify NuBCP-9 release from HGN-NuBCP nanoparticles, cell-free and cell-based release studies were conducted. Up to 22% of loaded peptide was released from NuBCP-9 loaded HGN nanoparticles when 500mW 800nm laser was applied for 15 seconds (Figure 4.3C). Fluorescence of Cy5 tagged peptide after KCN etch washing of HGN-NuBCP pellet was used to calculate total peptide loading (Figure S6). Exposure of HeLa cells to HGN-NuBCP nanoparticles resulted in internalization of the particles and could be seen as florescent puncta within the cells (Figure 4.3D). After NIR irradiation, nanoparticle and endosomal release could be seen as both FAM-DNA and NuBCP-

Cy5 could be seen as puncta diminished and dyes diffused within the cytosol (Figure 4.3.D).

To determine if HGN delivery of NuBCP-9 could decrease cancer cell viability, MDA-MB-231 breast cancer cells were exposed to HGN-NuBCP and irradiated with a NIR laser. After 96 hours post laser exposure, HGN-NuBCP treated cells had an 80% loss in cell viability and no loss in cell viability was seen for 3μM NuBCP peptide treated cells, demonstrating that HGNs are needed for cellular internalization (Figure 4.3E). Laser irradiation of HGN only controls in MDA-MB-231 cells resulted in around 20% loss in cell viability. This is most likely due to cellular heating as NIR irradiation of the HGN nanoparticles results in heat transfer. Binding of NuBCP-9 to Bcl-2 causes Bcl-2 to transform from pro-survival protein to an apoptosis inducing protein via mitochondrial permeabilization. To validate that laser irradiation of HGN-NuBCP treated cells was inducing permeabilization, JC-1 mitochondrial staining was done on HGN-NuBCP treated and laser irradiated H460 lung cancer cells. In cellular studies, aggregated JC-1 dye disassociates into a green fluorescing monomeric form when the mitochondrial membrane depolarizes. Mitochondrial depolarization can be an early indicator of cell death due to apoptosis. Thirty minutes after laser irradiation, confocal images exhibit dispersal of NuBCP-Cy5 puncta and increase JC-1 green fluorescence, indicating mitochondrial permeabilization (Figure 4.3F). Increased green fluorescence was only observed in laser irradiated areas, confirming the mitochondrial membrane becomes destabilized after irradiation of cells with HGN-NuBCP. There was no effect of HGN alone with laser irradiation (Figure S7). Together, these data demonstrate HGN-NuBCP's ability to enter the cell, allowing laser cargo release and resulting in apoptosis induced cell death.

To demonstrate the *in vivo* efficacy of this HGN-NuBCP approach, we exposed fluorescently stained PacR H460 cells to either vehicle, HGN, or HGN-NuBCP and transplanted them into zebrafish embryos (Figure 4.4A). The transplanted cells were imaged before and 3 days after two-photon NIR laser irradiation to measure loss of PacR H460 cells within the zebrafish. Half the zebrafish from each group were withheld from irradiation as controls. NIR irradiation had no

effect on zebrafish survival as 98.3% and 96.6% of non-irradiated and irradiated zebrafish survived respectively. Laser irradiation of HGN-NuBCP treatment group had the greatest effect on the growth of PacR H460 cells inside zebrafish. Three days after laser irradiation, average PacR H460 xenograft tumor growth was reduced by 56.4% compared to the non-laser control for HGN-NuBCP treated groups (Figure 4.4D,G). PacR H460 xenograft growth was not significantly affected by HGN alone (Figure 4.4C,F). Laser induced cell reduction with HGN exposure is similar to what was seen *in vitro* experiments where HGN irradiation may be generating localized heating. Our model displays the potential application of HGN-NuBCP as a therapeutic to combat chemoresistant cancers as laser irradiation posed no harm to non-HGN-NuBCP exposed host and significantly reduced PacR H460 growth after 3 days.

4.3.4. *New Bcl-2 Function Converter Compounds*

To diversify our efforts in discovering potential BFC drugs, our lab has also tested small molecule compounds for similar Bcl-2 function converting capabilities as NuBCP-9. *In vitro* screening resulted in several promising compounds, BFC1101, BFC1103, BFC1108 and BFC1111. These compounds successfully reduced cell viability in both PacR and parental H460 cell lines, but had greater effects in PacR H460 cells, correlating with increased levels of Bcl-2 expression (Figure 4.5A,B). Zebrafish provide an ideal model for testing compound toxicity as embryonic-larval zebrafish are sensitive to the environment and can be easily exposed to compounds by addition to fish media in minimal volume, thus using conserving often precious amounts of compound. Zebrafish survival to BFC compounds at concentrations of 10, 20 and 30μM was conducted over 4 days of continuous treatment on 3 to 7 dpf larvae. Only BFC1103 demonstrated toxic effects to larval zebrafish as no larva survived the 4-day treatment at 30μM concentration (Figure 4.5C). Toxic effects were also seen at 10μM as only 60% of larva survived with a number of surviving zebrafishes displaying cardiac and yolk sac edema. All other BFCs, including 0.5% DMSO control, had 90% or more larva survive for all concentrations.

To test BFC compounds ability to reduce cancer growth *in vivo*, PacR H460 cancer cells were fluorescently dyed and transplanted into the yolk of embryonic

zebrafish. PacR H460 injected zebrafish were then exposed to either vehicle, 30µM BFC1101, 20µM BFC1103, 20µM BFC1108 or 20µM BFC1111 for three days by addition of treatment to fish media. Survival of larva was similar to what was seen in toxicity testing as there was increased death with BFC1103 treatment, but not other treatments. Confocal images of the fluorescent cells taken before treatment and after three days of treatment, display xenografts with pronounced decreases in PacR H460 mass for BFC1101, BFC1103 and BFC1108 treatment compared to vehicle controls (Figure 4.5D). Image analysis of injected cancer cells confirms a significant decrease in cancer masses for BFC1101, BFC1103 and BFC1108 compounds as cancer presence was by reduced three to four times compared to vehicle (Figure 4.5E).

To verify that the compounds BFC1101 and BFC1108 were effective in other cancer types, the BFC compounds were tested on triple negative breast cancer MDA-MB-231 cells. Two MDA-MB-231 cell lines with different Bcl-2 expression levels were tested. Bcl-2 high MDA-MB-231 cells were transfected with Bcl-2 plasmid while Bcl-2 low MDA-MB-231 cells were transfected with a pcDNA control vector. Western blots for Bcl-2, reveal increased Bcl-2 protein presence in Bcl-2 high MDA-MB-231 cells (Figure 4.6A). Treatment with BFC1101 and BFC1108 on both MDA-MB-231 cell lines resulted in a significant decrease in cell viability for Bcl-2 high cells where viability was reduced to 37% and 29%, BFC1101 and BFC1108 respectively, after 72hrs of treatment (Figure 4.6B,C). Compounds were further tested with our zebrafish xenograft assay. As with the PacR H460 xenografts, zebrafish survival was not affected by BFC treatment (data not shown). Image analysis of pre- and post-treatment revealed BFC compound effects for both Bcl-2 low and high xenografts, but effects were not significant compared to controls. However, when both Bcl-2 low and high xenograft data were combined, there was a significant difference between the controls (Figure 4.6.D). Representative images of pre-treatment and post-treatment xenografts display strong compound effect was many xenografts exhibited large decreases in cancer mass (Figure 4.6E). While Bcl-2 low MDA-MB-231 cells have lower expression of Bcl-2, they are not devoid of Bcl-2 protein. It is possible that in an *in vivo* environment lower Bcl-2 is sufficient for

BFC1101 and BFC1108 to elicit a robust effect. More experiments must be done to determine the extent of Bcl-2 expression needed for BFC induced apoptosis *in vivo*.

4.4. Discussion

Here we present multiple promising Bcl-2 targeted cancer therapeutic drugs. They are capable of converting Bcl-2 from a pro-survival protein into a pro-death protein. Bcl-2 is a targetable protein involved in a specific cellular pathway that can be crucial to cancer cell survival [79]. Bcl-2' overexpression promotes cell survival in many cancers through overexpression. Bcl-2 overexpression provides a possible means to specifically destroy cancer cells, sparing healthy cells and reducing negative side effects. However, Bcl-2 is not easily targetable as it resides within the cytosol and is not exposed to the extracellular environment.

Biologic drugs, such as peptides, have the potential to revolutionize cancer therapy. Their low toxicity and high specificity are essential attributes in the design of drugs [86]. Mechanisms of delivery must be addressed, however, in order to reveal their true potential. Here we provide a novel light-directed delivery mechanism to effectively treat Bcl-2 overexpressing cancers. By attaching NuBCP-9 to hollow gold nanoparticles, we have developed a drug capable of entering the cell, releasing NuBCP-9 into the cytosol and initiating apoptosis. Peptide delivery is hampered by lack of endosomal release and therefore increased concentrations are needed for desired effects [98]. Increased concentrations, however, often lead to decreased specificity. Our research addresses this problem by laser activated endosomal release of peptide. The result is an increase in potency as cytosolic release is in the nanomolar scale compared to other peptide deliveries in the micromolar scale. Furthermore, laser release allows for location specific delivery, mitigating potential problems of systemic release on healthy tissues. This therapeutic problem cannot be understated as current systemic deliveries are limited to patients that can most likely withstand the adverse side effects as they can irreparably harm health compromised individuals [99,100].

We demonstrated that our HGN-NuBCP drug can be successfully released inside a living animal by laser activation. While nanoparticle treatment was less

effective *in vivo* than *in vitro,* it is promising that a significant decrease in cancer growth was seen in a living animal. Cells treated *in vitro* not only had maximal peptide exposure, but also benefited from the lack of *in vivo* environment during treatment. Induction of apoptosis *in vitro* and *in vivo* manifest at different time scales (hours compared days) as the *in vivo* environment can protect against cell death [48–50]. If the nanoparticle light-delivery experiment were able to be extended, perhaps stronger effects could have been seen. Furthermore, it is significant that zebrafish were not affected by laser activated treatment. Our zebrafish xenografts were capable of undergoing NIR laser treatment without any damaging effects to exposed tissue or effects from treatment release. This exemplifies the potential impact that laser release of NuBCP-9 could have on patients as it could allow for increased treatments without the damaging side effects of most cancer treatments.

Zebrafish offer a significant advantage to researchers in drug discovery as they can provide early signs of toxicity as well as *in vivo* effectiveness. In early development, zebrafish are highly sensitive to environmental compounds and therefore have been adopted by researchers to test for potential environmental impacts [36]. Early *in vivo* testing is beneficial as it provides researchers the ability to gain confidence in potential drugs before committing to expensive and time-consuming rodent models [63]. Zebrafish testing could reduce unnecessary expenses and time spent on toxic or ineffective drugs. We demonstrated the ability to successfully test small molecule compounds in an embryo-larva model to identify two compounds that reduce cancer growth *in vivo* without harm to the zebrafish. With this model, we were able to eliminate two compounds that were successful *in vitro* cell-based assays but failed to produce results in zebrafish xenografts or caused harmful damage to the host. Furthermore, we were able to gain increased confidence in BFC1101 and BFC1108 compounds by testing on an additional cell line expressing significant Bcl-2 in our zebrafish model and displaying decreased cancer growth. Treatment with these compounds occurred by exposure within the fish media, displaying good bodily absorption and ability to penetrate into tissue. Additionally, zebrafish xenograft experiments occurred over the course of 3 days of treatment, highlighting the effectiveness of the compounds to quickly reduce cancer growth.

There are opportunities for zebrafish to become increasingly useful as an *in vivo* model to study cancer therapeutics. Patient derived xenografts provide a more authentic view to cancer in an individual compared to immortalized cancer lines. Like mouse models, zebrafish can be a host for patient tumor cells and tissues. Zebrafish patient-derived xenografts have been shown to display similar cancer behavior as seen in the cancer patient. For instance, transplanted bone metastasis tumor cells from a patient with breast cancer were seen migrating to caudal hematopoietic tissues, comparable to human bone morrow, in zebrafish xenografts [101]. Transplantation of whole patient tissue was also demonstrated with pancreatic tumor tissue where it implanted into the yolk of embryonic zebrafish and displayed similar metastatic behavior seen in the patient [12]. Zebrafish are not only capable of harboring patient cancer cells and tissue but are also capable of transforming how doctors treat cancer patients by personalizing medicine. In order to select proper drug treatment for an individual, biopsy samples could be processed and transplanted into zebrafish in the same manner described here. As zebrafish embryo-larva require a minimal number of cancer cells, many more xenografts could be generated from a single patient than traditional murine models. With numerous different xenografts, many different treatments could be tested with results produced within weeks. This model has the potential to provide doctors with personalized experimental data on drugs before treatment has even begun. The rapid ability to generate this personalized data has the potential to greatly extend patient lifespan as patients with aggressive cancers need appropriate treatment quickly and do not have months to find the best treatment.

4.5. Materials and Methods

Cell culture

Cell lines were obtained from ATCC (ATCC, Manassas, VA, USA) and maintained according to manufacturer's instructions. The human lung cancer cell line NCI-H460 (ATCC) were cultured in RPMI medium (Corning, Manassas, VA, USA) containing 10% FBS (VWR Life Science, Radnor, PA, USA), 100 U/mL penicillin, and 100 mg/mL streptomycin (Corning). MDA-MB-231 and HeLa cell lines were

cultured as above except with DMEM medium, not RPMI medium. All cell lines were maintained at 5% CO_2 and 37°C. Paclitaxel resistant H460 cells were derived by treating cells once a week over 6 weeks, initially with 1 nM paclitaxel and then increasing dose incrementally up to 100 nM. Paclitaxel resistant H460 cells were derived over a period of 6 weeks. Once resistance was confirmed, paclitaxel was withdrawn from the cells. Resistance to paclitaxel was maintained without presence of paclitaxel measured up to 2 months. A parental line was maintained for a similar number of passages as the resistant line. H460 paclitaxel resistant cells were cultured in paclitaxel free media for a minimum of 3 weeks prior to all experiments. Bcl-2 overexpression was performed as previously reported with modifications [87]. MDA-MB-231 cells were seeded at a density of 1 x 10^6 cells per well in 6-well plates and incubated overnight. Cells were transfected the next day at 80-90% confluency with 2 µg of the pcDNA plasmid or Pcdna + Bcl-2 plasmid DNA using Lipofectamine 2000 transfection reagent (Thermo Fisher Scientific, Walktham, MA, USA). The transfected cells were grown under G418 selection with individual clones being isolated and expanded in the presence of G418.

Chemicals and peptides

Paclitaxel and doxorubicin were purchased from Sigma Aldrich (St Louis, MO, USA). DMSO was purchased from VWR Life Sciences (Radnor, PA, USA). Cell penetrating NuBCP-9, NuBCP-9/AA was purchased from Lifetien (Lifetien, Hillsborough, NJ, USA) [30].

Viability assay

Cells of interest were plated at 2000 cells per well in 96-well black tissue culture plate and allowed to adhere to the plate overnight. Viability assays were performed using 10% serum medium unless otherwise stated. Drugs were diluted in supplemented tissue culture medium and added at increasing concentrations, with DMSO as a vehicle control. Cells were then incubated for either 48 hour or 72 hours in presence of the compound, Promega Titer Glo (G7570, Promega, Madison, WI) was added to the wells at the assay end point according to manufacturer's protocol. Luminescence was measured using Tropix TR717 Microplate luminometer. Percentage of viable cells is relative to vehicle (100%).

Western blotting

Analysis of protein abundance was performed by Western blot according to standard techniques. Briefly cell lysates were collected using RIPA buffer with protease inhibitor, and then quantified using BCA assay. Some cell lysates were collected using 2X Laemmli buffer directly. Samples were boiled for 5 min and ran on SDS PAGE 12% and transferred to PVDF membranes by semi-dry transfer. Blots were probed using following antibodies, Bcl-2 (sc-509, Santa Cruz Biotechnology, Dallas, TX, USA), GAPDH (sc-365062, SantaCruz), Cleaved Caspase 3 Asp175 (9661, Cell Signaling, Danvas, MA, USA). Chemiluminescence signal was developed using horse radish peroxidase conjugated secondary antibodies (SouthernBiotech, USA) and SuperSignal West Pico reagent (Thermo Fisher Scientific, Waltham, MA, USA). Images were captured using a G:BOX imaging system and GeneSys software version 1.5.9 (Syngene, Cambridge, UK).

Annexin V for apoptosis using flow cytometry

Cells were seeded into 6 well tissue culture plates to give approximately 50% confluence and allowed to attach overnight. The cells were then treated for a period of time indicated in figure legend with the appropriate compound at various concentrations. An annexin V-conjugate PerCP-eFluor 710 apoptosis detection kit was used as described by the manufacturer's protocol (88-8008, eBioscience, Waltham, MA, USA). Harvesting of cells included collection of floating and attached cells following trypsinization. Data were acquired using a CytoFLEX S flow cytometer (Beckman Coulter, Brea, CA) and 10,000 events on the PC5.5 channel were analyzed using CytExpert software (Beckman Coulter).

Bcl-2 BH3 conformation change assay

Cells were seeded at 10^6 per well in a 6 well plate and allowed to adhere overnight. The following day cells were treated with vehicle or indicated compound for 24 hours. Supernatant and attached cells were removed from plate using trypsin and washed 3 times in cold PBS. Cells were fixed with 3.7% PFA for 10 minutes at room temperature. Fixed cells were then washed with PBS and permeabilized using Triton x-100 0.1% in PBS for 10 minutes, this was followed by three PBS washes. Cells were then resuspended in Block solution (0.1%BSA in PBS) for 1 hour at room

temperature. Primary antibody Bcl-2 BH3 domain specific (cat# AP1303a) (Abgent, San Diego, CA) was added at a 1:30 dilution overnight at 4°C and then washed three times using cold PBS. For control experiment primary antibody Bcl-2(100) (cat# MA5-11757) (Thermo Fisher Sci, Waltham, MA, USA) was added at 1:50 dilution overnight at 4°C and then washed three times using cold PBS. Secondary antibody FITC conjugate was added at 1:100 dilution in block solution for 1 hour at room temperature. Samples were analysed using flow cytometry, shift of peak to the right in FITC channel determines extent of Bcl-2 BH3 exposure.

Zebrafish Xenografts and Two-photon Laser Exposure.

Zebrafish (Danio rerio) were housed at the Sinnhuber Aquatic Research Laboratory at Oregon State University in accordance with Institutional Animal Care and Use Committee protocols. Adult 5D Tropical zebrafish were maintained under standard laboratory conditions of 28±1°C on a 14hr light/10 hr dark photoperiod in fish water consisting of reverse osmosis water supplemented with a commercially available salt solution (0.6%, Instant Ocean, UnitedPet Group, Inc., Blacksburg, VA, USA). Collected eggs were staged according to Kimmel *et al* [6]. At 24 hours post fertilization (hpf), zebrafish embryos were maintained in E3 media with phenylthiourea (0.003%, Sigma, USA).

Xenograft transplantation protocols were adapted from Lal *et al* [17]. Briefly, cancer cells were labeled with a CM-DiI dye (Thermo Fisher Sci.) according to the manufacturer's protocol and suspended to a concentration of $2x10^7$ cells/mL. Cell suspension was loaded into a borosilicate glass needle pulled from a pipette by a micropipette puller (Sutter Instrument, Novato, CA). Approximately 200 cells were transplanted into the yolk of 48hpf embryos by air-driven micro-pressure injector as described in Lal et al. After transplantation, embryos recovered overnight at 34°C without light.

For nanoparticle experiments, cancer cells were labeled with a CM-DiI cell tracker dye (Thermo Fisher Sci.) according to the manufacturer's protocol and exposed to vehicle (media), HGN 3.2 pM or HGN-NuBCP 3.2 pM loaded with 10 μM NuBCP treatment. Cells were allowed to incubate with treatment at room temperature for 1hr on a rotator. Cells were then washed with PBS and suspended in

DMEM to a concentration of $2x10^7$ cells/mL for transplantation. For two-photon laser irradiation, zebrafish were immobilized by being anesthetized by emersion in 0.2mg/mL Tricaine E3 media and imbedded in 0.8% (w/v) low melting point agarose on a glass bottom 96-well plate. Zebrafish were irradiated using a mode locked Ti:Sapphire Laser widely tunable femtosecond pulsed laser (140 fs pulse duration, 80 mHz repetition rate, Chameleon Vision Laser, Coherent) using a Zeiss LSM 780 confocal microscope at 20x objective. Zebrafish yolks were irradiated at 800 nm, 6% NIR laser power and in 0.75 nm slices throughout the yolk volume.

For imaging, zebrafish xenografts were anesthetized by emersion in 0.2mg/mL Tricaine E3 media and imbedded in 0.8% (w/v) low melting point agarose on a glass bottom 96-well plate. A Zeiss LSM 780 confocal microscope with a 10x objective was used to capture fluorescent cells at 1 and 4-day post injection (dpi). Images were captured as z-stacks with wide-field settings. H460 cancer growth was analyzed using Fiji (Fiji is Just ImageJ) software [66]. Images were processed by making a maximum projection image of the z-stack and using a median filter. Cancer area was calculated by creating a binary mask from thresholds with the Otsu algorithm and calculating the total area of the resulting segmented objects. Increases in total area from 1 to 4dpi were considered cancer growth.

Hollow gold nanoshell synthesis and dialysis

HGNs were synthesized through a previously described galvanic replacement of silver seed particles (1). Briefly, the synthesis can be broken into three steps. The first step initializes the silver seed of the particle in a 500 mL solution of 0.2 mM $AgNO_3$ (Sigma) and 0.5 mM sodium citrate (Sigma) heated to 60 ˚C. 0.5 mL of 1.0 M $NaBH_4$ (EMD) was added quickly to reduce the silver solution to create the initial silver seed. The solution remained at temperature for 2 hours and then left to cool to room temperature. The second step of the synthesis grows the silver particle to the final 45 nm size by the addition of 0.75 mL of 2 M $NH_2OH•HCl$ (Sigma) and 1.75 mL of 0.1 M $AgNO_3$. The solution stirred overnight to allow for full growth of the silver particles to be used for template for later galvanic replacement. The third and final step in the synthesis is the galvanic replacement of the sacrificial silver template by the addition of 3.2 mL of 25 mM $HAuCl_4$ (Sigma) to the heated solution at 60 ˚C

to obtain hollow gold nanoshells ~45 nm in diameter with an absorption peak maximum at 750 nm. The HGNs were dialyzed overnight in sodium citrate buffer (500 mM) with 0.03 % diethyl dicarbonate (DEPC) (Biochemica) in dialysis cassettes (MWCO 20 kDa).

HGNs surface modifications

DNA absorption. Thiol-PEG-DNA-amine (C6-S-S-PEG18-5' ACCCTGAAGTTCATCTGCACCACCG 3'- NH2 (100 μM, Biosearch Technologies) was deprotected through a 20 minute incubation with 12.5 mM Tris(2-carboxyethyl) phosphine hydrochloride (TCEP,Sigma). A chloroform extraction was performed to remove the C6 cap on the 5' end of the oligo. 6 μM of TCEP treated DNA was added to 64 pM HGN. After a brief sonication, 10 mM sodium citrate was added to adjust the pH of the solution to 3.1 in order to allow for low pH DNA absorption onto the surface of the HGN. After 20 minutes of incubation at a low pH, the pH was raised to 7.4 with 1 M HEPES (Sigma) and the solution was slowly salted to 1M Na+ over a period of 20 minutes using 3.0 M sodium chloride (NaCl), 0.3 M sodium citrate (Na_3Cit) pH 7.0 (SSC 20x) with 0.01% Tween-20 and 1 mM $MgCl_2$. After another 20-minute incubation excess DNA was through two wash steps performed by centrifuging at 10,000 x g for 10 minutes with resuspension and sonication in washing buffer (1mM $MgCl_2$, 0.01 % Tween-20, 300 mM NaCl and 30 mM Na_3Cit pH 7). After the last wash, the particles were suspended in hybridization buffer (10 mM $MgCl_2$, 600 mM Na+).

Hybridization of complementary DNA. Complementary DNA (2 μM) is added to the HGN-DNA in ratio of 1:9 (5'-biotin to 5'-FAM labeled) to allow for a varied surface modification of the HGN. 0.2 μM Biotin and 1.8 μM DNAcomp-FAM are added to hybridization buffer, mixed and then added to 64 pM HGN-DNA to a final concentration of 1 μM complement DNA with 32 pM HGN-DNA and sonicated. The solution is then heated at 70 ˚C for 2 minutes and held at 45 ˚C for 30 minutes before washed two times with conjugation buffer (10 mM HEPES, 1mM $MgCl_2$ and 0.01% Tween-20).

NTA functionalization of HGN-DNA. N-[Nα,Nα-Bis(carboxymethyl)-L-lysine]-12-mercaptododecanamide (NTA) (Sigma) was added to the amine at the 3' end of the dsDNA strand through a 20-minute room temperature incubation with 1 mg/mL NHS-PEG4-maleimide linker (Quanta Biodesign). After 20 minutes the maleimide terminated HGN-DNA particles were washed three times at 4 ˚C and then suspended in conjugation buffer with 50 μM NTA, sonicated and left at room temperature for 3 hours and then washed three times in PBS with 0.01% Tween-20 (PBST).

Streptavidin and Biotin-TAT functionalization of HGN-NTA. An equal volume of 1mg/mL streptavidin (Prozyme) in PBST was added to 62 pM HGN-NTA and quickly sonicated and vortexed. After 1 hour of incubation at room temperature the streptavidin coated HGN were centrifuged twice at 10,000 xg for 10 minutes at 4 ˚C and each time was suspended in PBST. A final concentration of 20 μM biotin-TAT (Anaspec) was added in two steps of equal volume with a 30-minute incubation at room temperature after each addition. The particles were then washed another two times with PBST to remove any excess biotin-TAT and stored at 4 ˚C until further use.

NuBCP loading onto HGN and quantification of loading. NuBCP was loaded onto the HGN at 1, 3 and 10 μM initial concentration for 32 pM HGN and 500 μM $CuCl_2$ and incubated for 20 minutes on ice before being washed three times in PBST. Total loading per particle was determined through KCN etch. 32 pM particles were incubated in KCN solution (0.1 M KCN, 1 mM $K_3Fe(CN)_6$) to dissolve the gold particles and completely release the molecules coating the particle surface. In laser experiments, quantification of peptide released by laser was determined after centrifugation of the lasered sample and removal of the supernatant. The pellet was treated with KCN etch to determine the amount retained on the particle. Quantification of peptide in the supernatant and etched off the pellet was determined using standard linear calibration curves between concentration of Cy5 labeled NuBCP and the corresponding fluorescence intensity detected from the Tecan M200 plate reader. The fluorescence intensity in solution released with KCN etch or laser irradiation was converted to peptide concentration using the calibration curve.

Two-photon microscopy

Cells were plates 24 hours prior at 40,000 cells per well in an 8 well glass slide (Millipore cat no. PEZGS0816) in 200 μL of DMEM + 10% FBS. 500 uM $CuCl_2$ was added to 25 μL of ~32 pM HGNs (in PBST) prior to addition of NuBCP-Cy5. Particles were sonicated and incubated with 1, 3 and 5 μM NuBCP-Cy5 for 30 min on ice then spun down at 5,000 rcf for 10 min and washed 1X with PBST. HGN-NuBCP-Cy5 particles were then suspended in 200 uL of DMEM + 10% FBS and sonicated prior to addition to 8 well glass slide for 2 hours at 37˚C in 5% CO_2. Cells were washed 2X with PBS and then one drop of PBS was added to each well prior to cover glass addition. Samples were focused on using a 25 x water immersion objective lense and irradiated using a mode locked Ti:sapphire tunable femtosecond pulsed laser (100 fs pulse duration, 80 mHz repetition rate, Mai Tai HP, Newport-Spectra Physics). The excitation source was set to irradiate at 800 nm, 5% NIR laser power and in 0.69 nm slices throughout the cell volume. Images capturing FAM and Cy5 fluorescence were collected before and after laser irradiation.

Mitochondrial Depolarization Assay of H460 cells treated with HGN and HGN-NuBCP. Cells were plated and treated with HGN or HGN-NuBCP as described above. Prior to irradiation, cells were treated with media containing 10 μg•mL-1 solution of JC-1 dye (ThermoFisher) and incubated for 10 minutes. The cells were washed three times with PBS and treated with the laser conditions outlined above.

Femtosecond Pulse Laser Irradiation of HGN in MDA-MB-231 cells through Microcapillary Device. MDA-MB-231 cells were dissociated from flask using cell dissociation buffer (CDB, Gibco), and washed two times with PBS. 100,000 cells were suspended in media and incubated for 2 hours with HGN and HGN-NuBCP. The cells were washed two times with PBS and divided into 5,000 per tube in 100 μL and focused through a capillary tube positioned perpendicular to the NIR beam path at a rate of 100 μL•min-1. The samples were collected and plated on a 96 well plate and assayed for viability 96 hours later using the PrestoBlue viability stain according to the manufacturer's protocol on a Tecan M200 plate reader.

Data Analysis

Viability data were analyzed by one-way ANOVA with multiple comparison post-test using Prism software (Graphpad). Zebrafish xenograft cancer growth was assessed using JMP® Pro 13 (SAS) with Student's T Test. P values less than 0.05 were considered statistically significant.

4.6. Figures

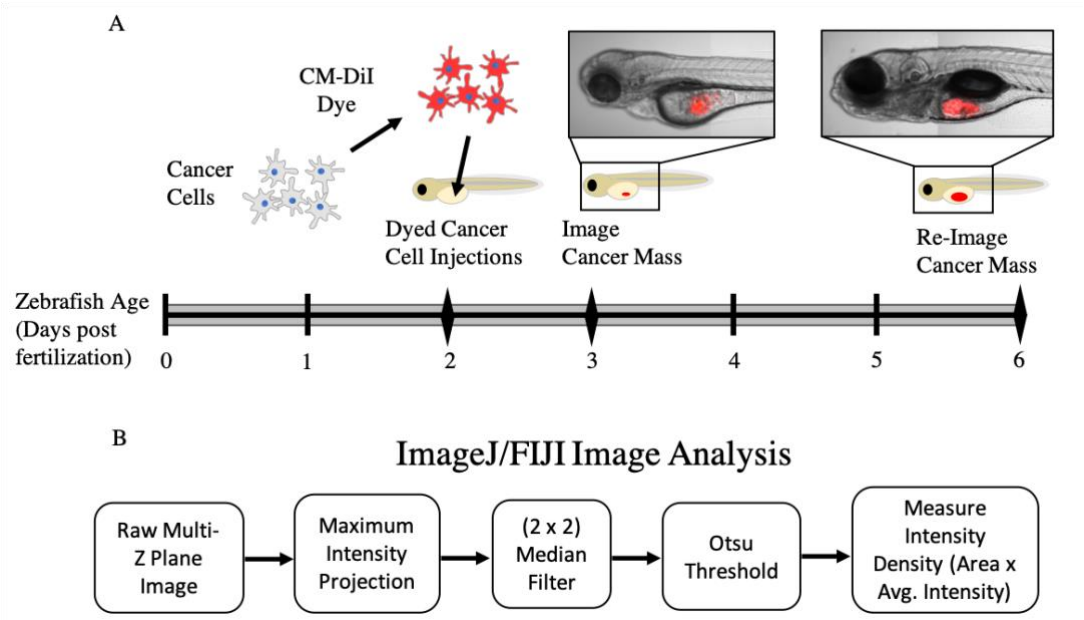

Figure 4.1. Embryo-Larva Zebrafish Xenograft Model. A) Diagram portraying xenograft assay. Cancer cells are dyed with CM-DiI and injected into the yolk of 2 days post fertilization (dpf) zebrafish embryos. After incubation overnight, 3dpf xenografts were imaged under a confocal microscope to assay the transplanted mass. Xenografts incubated at 33°C until being re-imaged for final cancer mass assessment. B) Image analysis workflow for xenograft assay using ImageJ/FIJI.

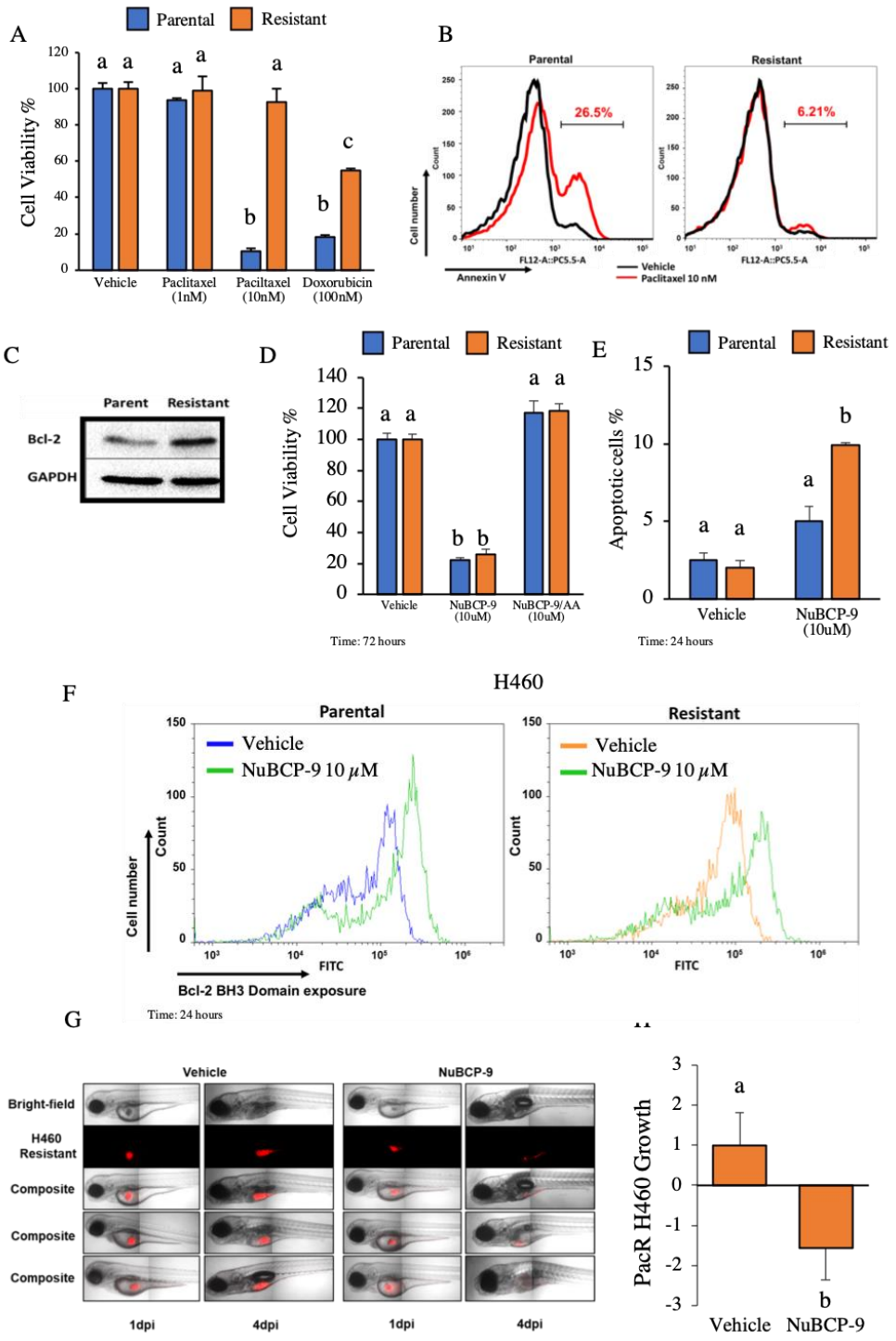

Figure 4.2. NuBCP-9 reduces paclitaxel resistant H460 cell viability and growth. A) Effect of paclitaxel and doxorubicin on H460 parental and derived paclitaxel resistant lung cancer cells after 72 hours of treatment. Percentage viability is calculated relative to vehicle treatment. Data is representative of three independent assays done in triplicate. One-way ANOVA with Dunnett's multiple comparisons

post-test: P<0.0001. B) Annexin V staining of H460 cells treated for 48 hours with vehicle or paclitaxel 10 nM. Histogram gate indicates percentage of apoptotic cells after paclitaxel treatment. Black line, Vehicle; Red line, Paclitaxel 10 nM. Results are the representative of three independent experiments. C) Western blot analysis of H460 parental and derived paclitaxel resistant cell Bcl-2 expression. D) Effect of NuBCP-9, NuBCP-9/AA (inactive form) on H460 parental and paclitaxel resistant lung cancer cells after 72 hours of treatment in 1% serum. Two-way ANOVA with Dunnett's multi comparisons post-test: P<0.0001. E) Annexin V staining of H460 parental and paclitaxel resistant cells treated with vehicle or 10 μM NuBCP-9 for 24 hours in 1% serum. Results are the mean ± s.d. of three technical replicates. Two-way ANOVA with Dunnett's multi comparisons post-test: P<0.001. F) NuBCP-9 induces conformational change in Bcl-2 and exposes its BH3 domain. Parental and Resistant H460 cells were treated for 24 hours with vehicle or NuBCP-9 (10 μM) and immunostained with Bcl-2 BH3 specific antibody. Shift of peak to the right indicates BH3 domain exposure in upper panel. No such shift with the Bcl-2 conformation independent antibody. G) Representative images of zebrafish xenograft and 4-day post injection (dpi). Red indicates dyed H460 resistant cells. H) NuBCP-9 suppresses growth of paclitaxel resistant H460 cells in a zebrafish xenograft model. Growth of H460 paclitaxel resistant cells in xenograft zebrafish model, pre-treated with vehicle or NuBCP-9 (10 μM) for 6 hours prior to injection into zebrafish. n= 34 for vehicle and n = 27 for NuBCP-9. Results are the mean ± SEM of two independent experiments. Students t-test, P<0.05.

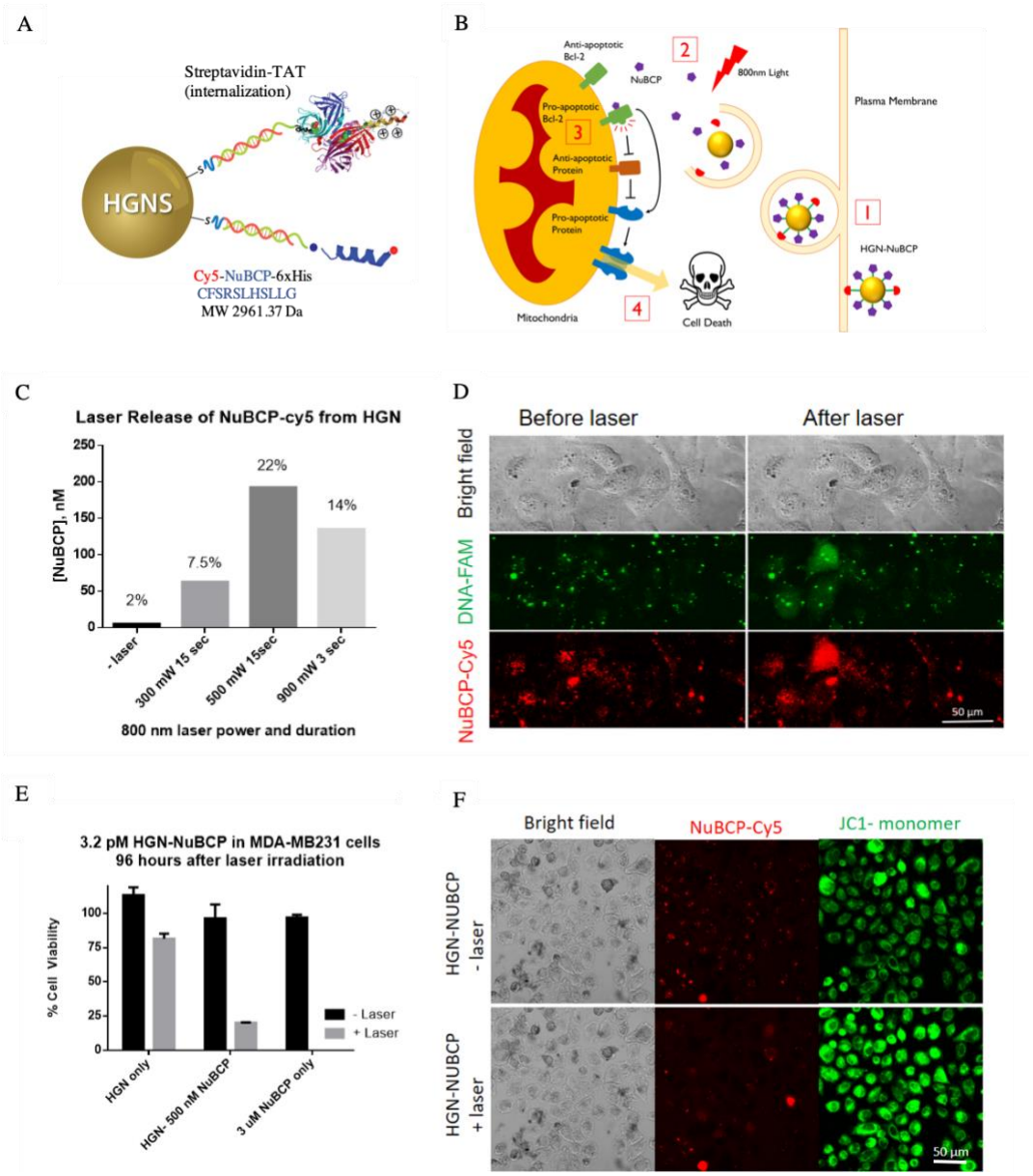

Figure 4.3. Hollow gold nanoparticle delivery of NuBCP. A) Orthogonal surface chemistry of internalization peptide Streptavidin TAT and therapeutic peptide NuBCP on a hollow gold nanoparticle (HGN). B) HGN-NuBCP delivery into cancer cell. (1) HGNs coated in NuBCP (purple hexagon) are taken into the cell by Streptavidin TAT (red semi-circle) mediated endocytosis. (2) Irradiation with 800nm light, releases NuBCP from HGN and endosome into the cytosol. (3) NuBCP binds to the Bcl-2 loop domain and converts Bcl-2 (green) into a pro-apoptotic protein which inhibits anti-apoptotic proteins (orange) and activates other pro-apoptotic proteins (blue) on the mitochondria. (4) Activated pro-apoptotic proteins facilitate

mitochondrial outer membrane permeabilization, initiating apoptosis, resulting in cell death. C) Increase in laser power correlates with NuBCP release from 3.2 pM HGN loaded with 900 nM NuBCP. Percent release is shown above bar graphs and determined by the percentage of peptide released into the supernatant after laser irradiation. D) Release of FAM labeled DNA and Cy5 labeled NuBCP in HeLa cells using two-photon microscope for NIR laser irradiation. Release of both DNA and peptide is shown from diffusion of dye labels throughout the cell after laser irradiation. E) Percent cell viability of MDA-MB-231 cells after treatment with 3.2 pM HGN, 3.2 pM HGN-NuBCP and irradiated with an 800 nm laser as cells flowed through a microcapillary tube at 100 μL/min. 500 nM and 3 μM NuBCP indicate the final concentration of NuBCP delivered in cell media via HGNs or in media alone for NuBCP only. Note the NuBCP only control was not treated with laser. F) Laser dependent release of NuBCP-Cy5 in H460 cells with JC-1 assay shows mitochondrial destabilization as green fluorescence increases from the JC-1 monomer upon irradiation with two-photon 800 nm laser.

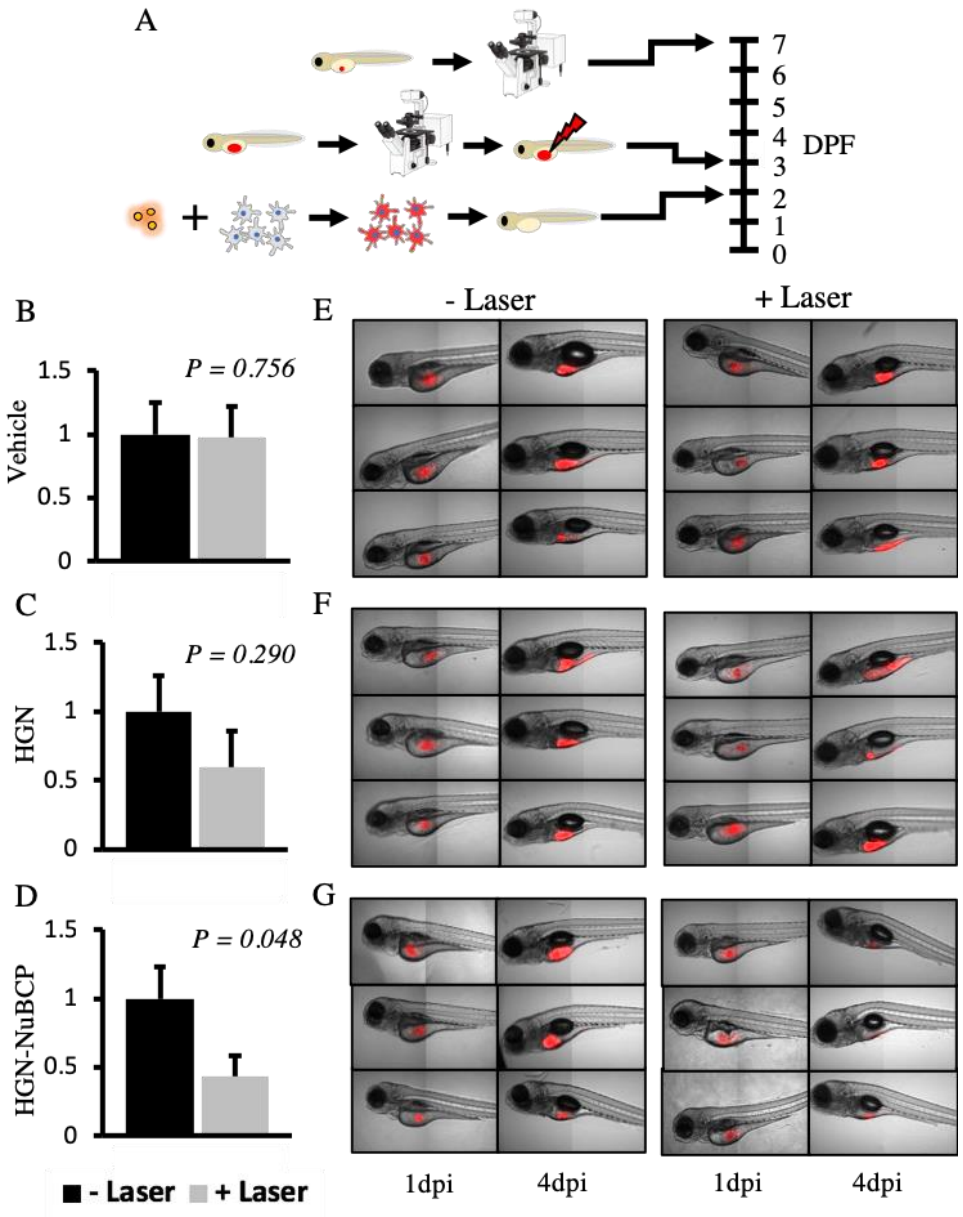

Figure 4.4. Two-photon laser induced release of NuBCP-9 results in reduction of H460 Paclitaxel resistant cells in zebrafish xenografts. A) Zebrafish xenograft scheme. H460 Paclitaxel resistant (PacR) cells were dyed with CM-DiI cell tracking dye, exposed to HGN-NuBCPs and then injected into the yolk of 2-day post fertilization (dpf) zebrafish embryos. The H460 PacR cells were imaged and then irradiated with a two-photon NIR laser within xenografts. Three days later H460 PacR cells were imaged again. Log2 fold change of cell area for vehicle (B), HGN

(C) and HGN-NuBCP (D) exposed H460 PacR cells in xenografts after no exposure -Laser or exposure +Laser to two-photon NIR laser. Data normalized to no laser control; Vehicle -Laser N = 20, +Laser N = 20: HGN: -Laser N = 20, +Laser N = 19. HGN-NuBCP: -Laser N = 19, +Laser N = 20. Representative figures zebrafish xenografts for vehicle (E), HGN (F) and HGN-NuBCP (G) treatment groups at 1and 4 dpi with transplanted H460 PacR cells (Red); 10x magnification.

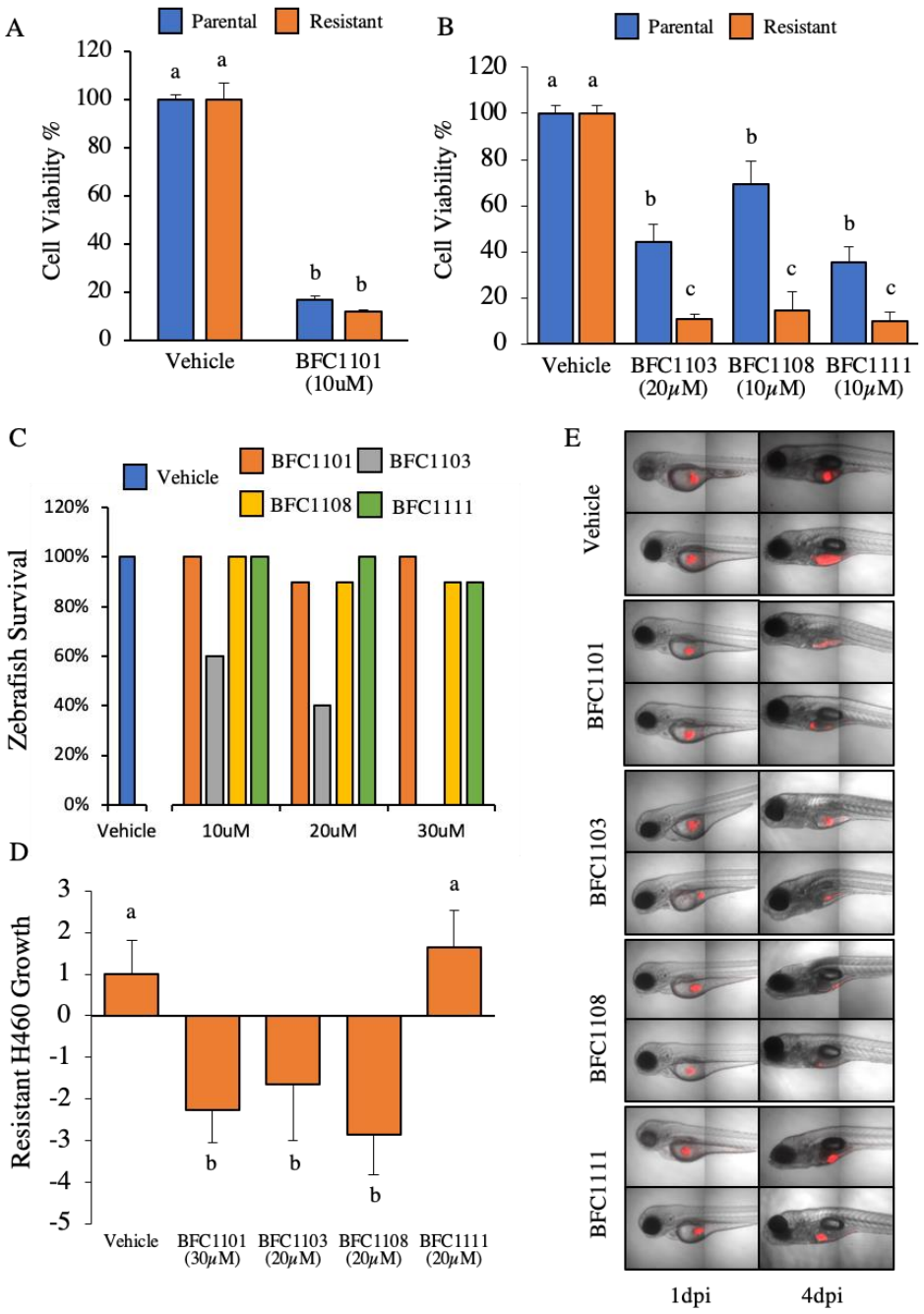

Figure 4.5. Small molecule Bcl-2 functional converters reduce H460 cell growth. A-B) Percent cell viability of parental and paclitaxel resistant H460 treated with (A)10μM BFC1101, (B) 20μM BFC1103, 10μM BFC1108, or 10μM BFC1111 relative to vehicle treatment. Data is representative of assays done in triplicate. One-way ANOVA with Dunnett's multiple comparisons post-test: $P<0.001$. C) Zebrafish 4-day embryo-larva survival for vehicle (blue) and treatment dose of 10μM, 20μM and 30μM for BFC1101 (orange), BFC1103 (gray), BFC1108 (gold), and BFC1111

(green). D) Growth of resistant H460 cells in zebrafish xenografts, treated with vehicle, 30µM BFC1101, 20µM BFC1103, 20µM BFC1108 or 20µM BFC1111. Vehicle $n = 25$, BFC1101 $n = 15$, BFC1103 $n = 8$, BFC1108 $n = 14$ and BFC1111 $n = 15$. Results are the mean ± SEM. Students t-test: $P<0.05$. E) Representative images of zebrafish xenograft 1 and 4-day post injection (dpi). Red indicates dyed resistant H460 cells.

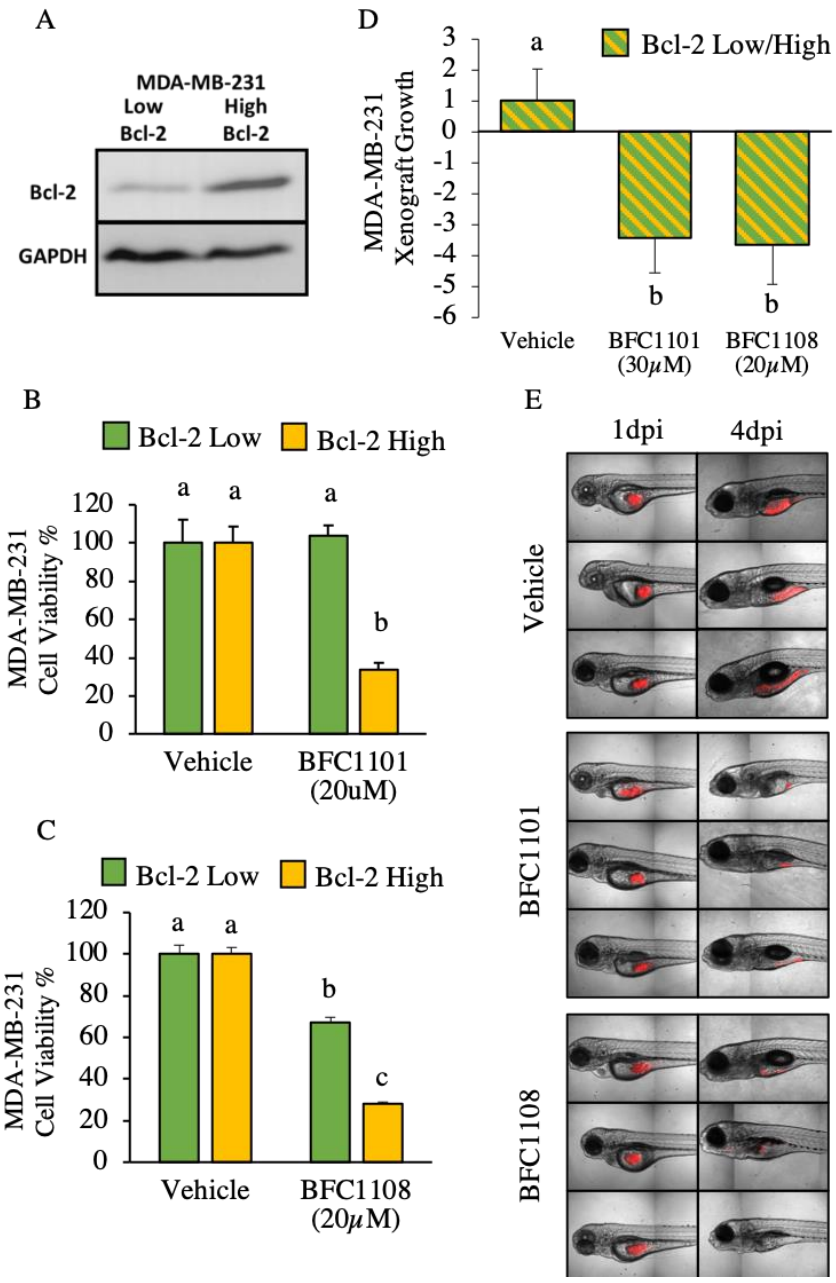

Figure 4.6. BFC1101 and BFC1108 treatment reduce MDA-MB-231 cell growth in zebrafish xenografts. A) Western blot analysis of MDA-MB-231 showing Bcl-2 expression in cells expressing Bcl-2 or control vector. B-C) Percent viability of MDA-MB-231 Bcl-2 low and high cells with vehicle and 20μM BFC1101 (B) or 20μM BFC1108 (C) relative to vehicle treatment. Data is representative of assays done in triplicate. One-way ANOVA with Dunnett's multiple comparisons post-test: $P<0.001$. D) Growth of MDA-MB-231 cells with either low or high Bcl-2 expression in zebrafish xenografts, treated with vehicle, 30μM BFC1101 or 20μM BFC1108.

Vehicle $n = 40$, BFC1101 $n = 40$, BFC1108 $n = 39$. Results are the mean ± SEM. Students t-test: $P<0.05$. E) Representative images of zebrafish xenograft 1 and 4-day post injection (dpi). Red indicates dyed MDA-MB-231 cells.

Chapter 5: Discussion

Author: John Gamble

5.1. Time-lapse Imaging with Zebrafish Xenografts

Time-lapse imaging can provide insights into cancer cell behavior and shed light on mechanisms necessary for migration, invasion, proliferation and metastasis. Zebrafish xenografts provides visual accessibility to an *in vivo* tumor-like environment. Using our zebrafish xenograft model, we were able to track individual GBM cell movement throughout the brain. Zebrafish encompass an ideal model for orthotopic research for studying brain cancer cell invasion. The zebrafish embryo-larva provide a small compact developed brain environment that can be captured in its entirety, something currently impossible in rodent models. Even with multi-photon technology, it is not possible to follow cells in a rodent brain as they can quickly infiltrate deeper into the brain further than infrared light can penetrate. Within the embryo-larva zebrafish brain, researchers can view the complete picture of GBM invasion. Our research showed that laminin alpha 5 affected U251MG cell invasion within the brain. Because we could account for the majority of the cells and their movements over the course of 10hrs, we discovered that laminin alpha 5 not only limited the number of invasive cells but also lowered the invasion rate of invasive cells. By identifying and categorizing cells based on movement, we were able to see differences within each subgroup. This provides significant information as it reveals that laminin alpha 5 reduced invasion throughout the brain and not only prevent U251MG cells from escaping the brain ventricle transplantation site.

Due to their small size and optical clarity, 3D images can be collected quickly to increase time resolution. In our study of laminin alpha 5 and its effects on U251MG cell invasion, we were able to quickly image 4 to 8 zebrafish xenografts per time-lapse experiment using a confocal microscope. This greatly increased our capacity to gather data and strengthened its statistical power. By increasing the number of xenografts per experiment, we provided better ability to see potential outliers within and between experiments. Variability in zebrafish offspring and variations during transplantation (i.e. amount of time cells spend in injection needle), could have a profound effect on how transplanted cells behave. Additionally, with the ease of gathering highly detailed images, our experiments were able to see invading

U251MG cell morphology. While we did not identify any differences in number or stability, U251MG cell pseudopodia were clearly distinguishable for most cells. Differences in pseudopodia could imply different modes of movement dictated by the surrounding extracellular matrix [102]. Capturing this detail in motion has the potential to uncover specific mechanisms required for cancer invasion and migration.

5.2. Need for Quantitative Data Analysis in Imaging

Zebrafish continue to be at the forefront of *in vivo* imaging due to their easy manipulability and high optically clarity. Using adaptive optics lattice light-sheet microscopy, Liu *et al* examined MDA-MB-231 migration through a zebrafish's blood stream in extreme detail [103]. Using their advanced microscopy technology, they captured a cancer cell tumbling through a blood vessel while nanoscopic long protrusions briefly adhered to the vessel walls. As imaging technology advances and images become more detailed and complex, quantitative image analysis must advance as well.

There is a great need for more quantitative cell biology [104]. Quantitation is necessary to remain objective so that we can understand the order and connect relationships between observable events. Without quantitation, we have few tools for interpretation of an image. We presented a number of different quantifiable measurements of GBM cell behaviors that can be gathered in an 3D *in vivo* environment. These quantitative measurements can provide standardization in the field, provide statistical confidence to data and help to remove potential bias from researchers. Moreover, by quantitating these cellular behaviors, we can assess differences that are not obvious to the eye. Alterations in cell behavior, particularly *in vivo,* can be nuanced, but still have substantial impact overall. With the aid of Tg(fli:EGFP)^{y1} zebrafish, we were able to capture blood vessel positions and identify instances of GBM-blood vessel interactions. Zebrafish blood vessels can be exploited by human glioma cell lines in a manner seen in both mouse models and human patients as glioma cells associate and migrate along vasculature as they invade brain tissue [17]. In order to examine if laminin alpha 5, a protein comprised in blood vessel basement membranes, affected U251MG cell blood vessel associations,

instances of association needed to be identified and categorized. By creating detection parameters and categorizing types of blood vessel associations, microtumor or individual U251MG cell, we were able to determine that laminin alpha 5 had no effect on U251MG cell association as instances were proportional to the occurrence of both individual and microtumor U251MG cells. This result was impossible to see without quantitation and was valuable as it indicated that laminin alpha 5 was not an influential attachment site on the basement membrane blood vessel for U251MG cells.

Computational analysis is integral to quantify the many aspects of cancer progression. Images can hold a wealth of information for researchers. Much of it might be hidden or unknown to researchers. Objects might be indistinguishable to a researcher as the human eye can only distinguish between 30 different shades of gray [105]. With 16-bit images having 65,536 different shades, software is needed to definitively detect minute differences in fluorescent intensity values. Furthermore, images processing can help to increase contrast for better object recognition. By performing contrast enhancement through histogram stretching and median filtering on time-lapse GBM cell images, the contrast-to-noise ratio was doubled and resulted in better cell tracking as more cells were identified per frame. Additionally, high-content imaging has the potential to generate large sets of imaging data. Zebrafish's conduciveness being a high-throughput model for cancer research is predicated on having automated image analysis. By using automated software like object recognition, automated image analysis allows researchers to mine images for data without having to commit many hours manually scanning images. In testing various potential cancer therapeutic drugs, we used automated ImageJ/Fiji software to analyze transplanted cancer area and intensity. Furthermore, this automated system allowed us to measure many different potential effects of treatment. While no significant differences were found, we were able to measure cancer dispersal and for instances of metastasis simultaneously with cancer growth. As more standardization and additional measurements are identified, algorithms can be updated to provide more data. Perhaps revealing subtle effects previously unseen.

5.3. Zebrafish as an Economical In Vivo Model

Zebrafish offer an *in vivo* model for researchers to conduct studies on human cancer. Zebrafish xenograft models are inexpensive compared to rodent models, in nearly every area of their care and maintenance. The larger the animal, the more cost is needed to feed, house and care for each individual. Zebrafish are relatively inexpensive to maintain and require a lot less space per animal than rodents. Additionally, zebrafish are easier to transport, particularly at the embryonic stage, and therefore encourage collaboration and sharing of transgenic lines without needing to recreate what has already been done. Individual labs can benefit from zebrafish core facilities as embryos can be transported to satellite locations with relative ease. To this effect, we have been able to conduct our zebrafish xenograft experiments at a fraction of the cost than that of traditional rodent models.

Our lab was able to efficiently evaluate potential novel cancer therapeutic compounds *in vivo*. With zebrafish xenografts, we were able to successfully test and validate different potential Bcl-2 functional converter drugs *in vivo*. These experiments provided valuable information of drug toxicity and effectiveness that will be used to prioritize for further *in vivo* testing. Additionally, we developed and demonstrated that a new nanoparticle light-delivery system was capable of therapeutic peptide delivery within an *in vivo* setting. The light-delivery system relied on 800nm light to cause release of the peptides from nanoparticle bonds and endosomal entrapment. While light-dependent release is straightforward in cell culture, fine tuning is needed to gain the same effects *in vivo*. Differences in power, duration and number of irradiations will be impacted as animal tissue induces light scattering but also provides survival factors to transplanted cancer cells such as growth factors. Zebrafish provided an economical means to test and fine tune irradiating procedures that could release the drug in cancerous cells while not harming healthy animal tissue. The more parameters that can be tested or established in zebrafish, the fewer mammalian subjects will be needed for further development.

5.1. Conclusion

Here we have demonstrated the strengths of the zebrafish xenograft model for its ability to provide *in vivo* human cancer data. Using zebrafish, we developed methodology for tracking and gathering quantitative data for glioblastoma (GBM) movement in a brain environment. Moreover, detailed images were captured of GBM cells and blood vessels using Tg(fli:EGFP)^{y1} zebrafish allow us to analyze GBM cell and vascular interactions. Using zebrafish, we successfully verified potential new Bcl-2 functional converting drugs that induce apoptosis in Bcl-2 dependent cancers. Additionally, we demonstrated a new nanoparticle light-delivery mechanism for delivering therapeutic peptides to tumor cells inside an organism. Our experiments not only demonstrate the capabilities of zebrafish for investigating cancer progression but also display their feasibility as an *in vivo* model for testing new cancer therapeutics.

Supplementary Figures and Tables

Primer	**Sequence**
EF-1α forward	GTGCTGTGCTGATTGTTGCT
EF-1α reverse	TGTATGCGCTGACTTCCTTG
lama5 exons 59–62 forward	GACATAGTGAACAGCATCTCAGCAGC
lama5 exons 59–62 reverse	GAGTCACTGCCATGTACTCCTTACTGG
lama5 5′ forward	GTAACCCAGCAGGTTCTGTTCATAATGAC
lama5 5′ reverse	GAAGAATCCATCCTTGCACACGTTACAGG

Table S1: Forward and reverse primers. Primers used for verification of lama5 truncation of mRNA.

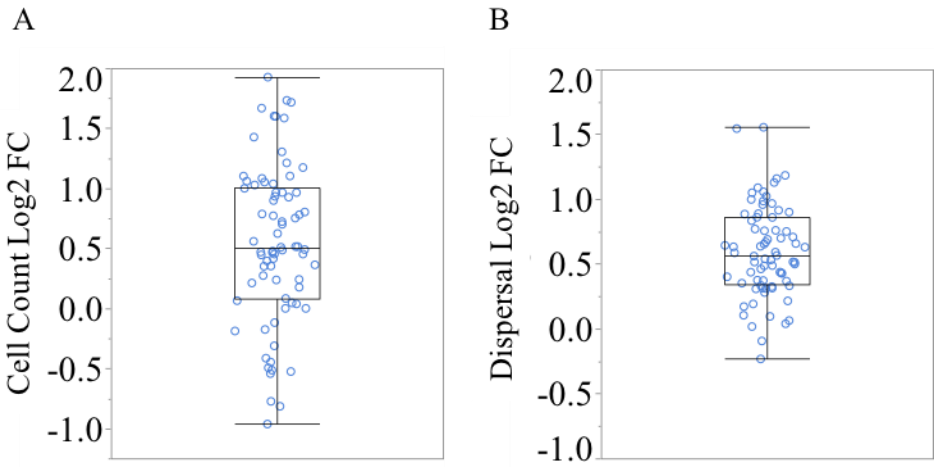

Figure S1. Increase in U251MG Cell Count and Dispersal in Zebrafish Xenografts. A-B) Box plots displaying the log2 fold change of cell count (A) and dispersal (B) of transplanted U251MG cells for each control larva (blue circle) after 3 days of incubation in a zebrafish brain.

Exon 59

GACATAGTGAACAGCATCTCAGCAGCTAAGAGTGCGGTGGAGCAGGCTA
ACAACACGGTGGCTAACGTTAGCGGTGTGCTGGCTCCAATTCAGAAGCAG
CTGGAGGAATGGCAGAAGCAGTACGGAGACTCCAACGCCACTAGTGAGG
ATATCAACAAAGCCCTCAATGACGCCAACACATCAG

Exon 60

TGGCTGCACTGAGCGACACTCTTCCTAAGCTGATAAAGAAGTTGGATCGC
CTGCACAACACCACGTTTCAGCCGTCCAACATCTCCGACAGCATCCAGAG
GATTCGTCAACTCATTGAGCAAGCACGCAATGCTGCCAACAAG

Inserted section of Intron 60-61

gtgccaactaagcgttttcccgtctaatctgttatagagttagttcacgataaaatgagcattctgttattattgtttatcttcaaatc
acaaatgaagatattttagattaaatttgagagctccctcatcctccatatacagcagtggttccaagatgttcaaagtccaga
aaaggaacaaaaacattgtcaaaacatgatctgacat

Exon 61

GTCAGCGTGTCAATGCAGTTTAATGGTAAATCGGGAGTACAAGTGAGGAC
ACCCAGTAATGTGGCAGACCTGGCAGCCTATTCATCACTCCAAATGTACA
TCAAGCTTCCCAGTCCTACCATTAAAAAGAAACGACAAACTGAAGCCACC
AACCCCCAGTTTGTCCTCTATCTTGGAAACCGAGAC

Exon 62

TCCAGTAAGGAGTACATGGCAGTGACTC

Figure S2. cDNA sequence from mRNA lama5 KD transcript showing cryptic intronic splice introducing premature stop-codon. Sanger sequencing results of laminin alpha 5 knockdown in zebrafish embryos using forward and backward DNA primers (highlighted magenta) for laminin alpha 5 exons 59 – 62 show insertion of intronic RNA resulting in premature stop-codon (highlighted red).

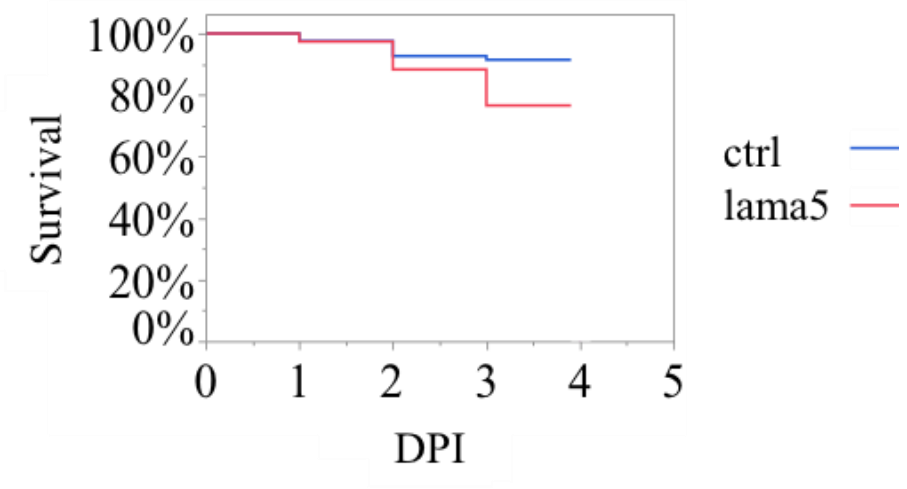

Figure S3. Zebrafish Xenograft Survival. Survival of zebrafish xenografts embryo-larva days post injections (DPI) for controls (blue line) and lama5 morphant (red line).

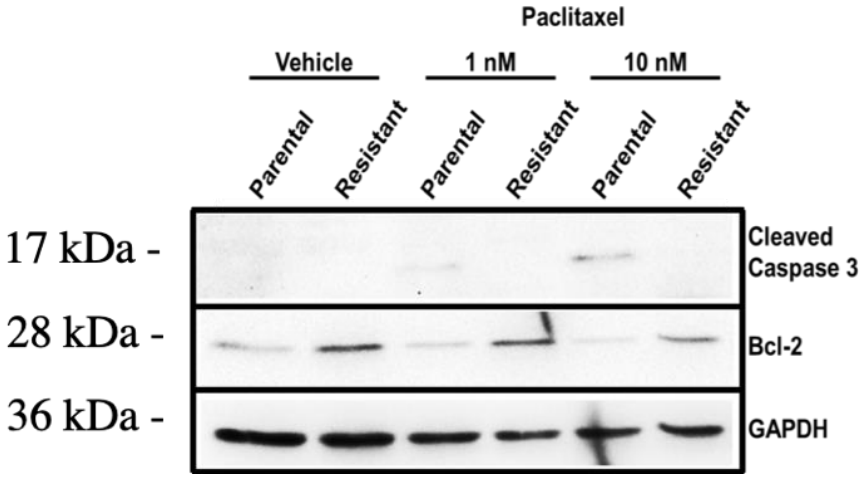

Figure S4. Paclitaxel resistance increases Bcl-2, preventing apoptosis. Correlation of high Bcl-2 and increased resistance to paclitaxel. Western blot analysis of H460 parental and paclitaxel resistant cells treated with paclitaxel for 48 hours and probed with indicated antibodies.

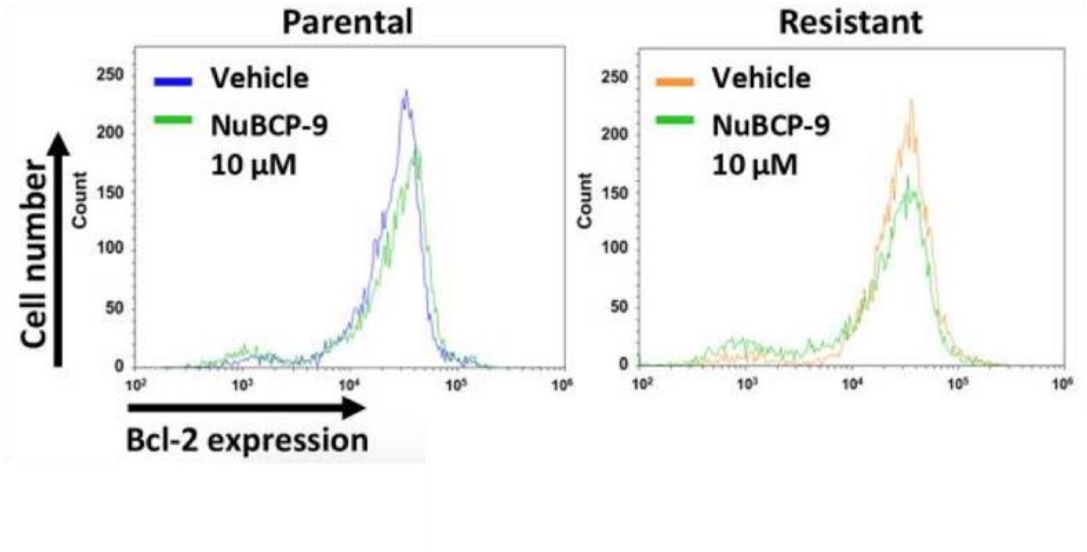

Figure S5. NuBCP-9 induces conformational change in Bcl-2 and exposes its BH3 domain. Parental and Resistant H460 cells were treated for 24 hours with vehicle or NuBCP-9 (10 µM) and immunostained with Bcl-2 conformation independent antibody and analyzed by flow cytometry. No shift is seen with conformation independent antibody.

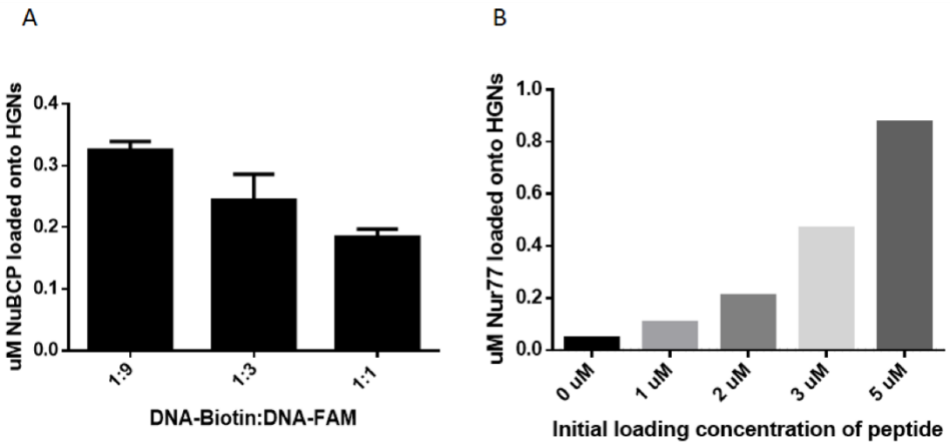

Figure S6. Optimization of NuBCP Loading onto HGNs. A. Ratio of Biotin:FAM complement strands on HGN-STV-TAT particles determines 1:9 particles allow for maximal loading of NuBCP with 3 μM initial peptide concentration. B. Increase in loading of NuBCP-Cy5 on 3.2 pM particles with increasing initial concentrations of NuBCP. NuBCP loading is determined by Cy5 fluorescence in KCN etch of washed HGN-NuBCP pellet.

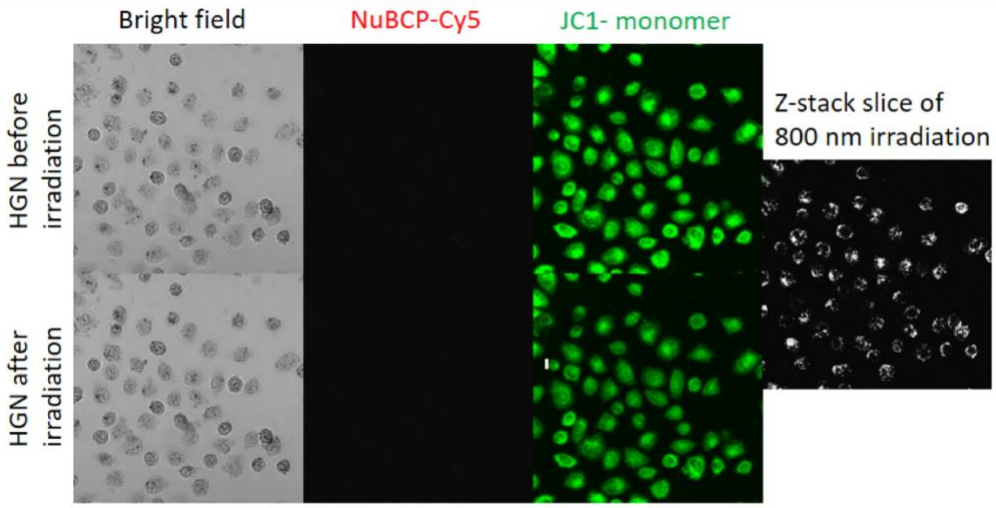

Figure S7. Irradiation of H460 cells without NuBCP in the presence of HGN does not cause mitochondria depolarization. Irradiation of HGN in H460 cells with JC-1 assay does not show an increase in green fluorescence from the JC-1 monomer upon laser irradiation with 800 nm laser equipped two-photon microscope indicating the mitochondria membranes remain intact post laser irradiation without NuBCP on the HGNs. No fluorescence is observed in the Cy5 channel due to no peptide on the HGNs. Confirmation of particles in cells through Z-stack slice of 800 nm irradiation which shows the surface resonance light scattering produced by the HGN internalized in the H460 cells. The white resonant light scattering is demonstrated through the white puncta visualized throughout the cells in the Z-stack slice during 800 nm irradiation.

Bibliography

[1] S. Breslin, L. O'Driscoll, The relevance of using 3D cell cultures, in addition to 2D monolayer cultures, when evaluating breast cancer drug sensitivity and resistance, Oncotarget. 7 (2016) 45745–45756. doi:10.18632/oncotarget.9935.

[2] L. Hui, Y. Chen, Tumor microenvironment: Sanctuary of the devil, Cancer Lett. 368 (2015) 7–13. doi:10.1016/j.canlet.2015.07.039.

[3] T. Sethi, R.C. Rintoul, S.M. Moore, A.C. MacKinnon, D. Salter, C. Choo, E.R. Chilvers, I. Dransfield, S.C. Donnelly, R. Strieter, C. Haslett, Extracellular matrix proteins protect small cell lung cancer cells against apoptosis: A mechanism for small cell lung cancer growth and drug resistance in vivo, Nat. Med. 5 (1999) 662–668. doi:10.1038/9511.

[4] G. Venugopalan, D.B. Camarillo, K.D. Webster, C.D. Reber, J.A. Sethian, V.M. Weaver, D.A. Fletcher, H. El-Samad, C.H. Rycroft, Multicellular Architecture of Malignant Breast Epithelia Influences Mechanics, PLoS ONE. 9 (2014) e101955. doi:10.1371/journal.pone.0101955.

[5] K. Stoletov, H. Kato, E. Zardouzian, J. Kelber, J. Yang, S. Shattil, R. Klemke, Visualizing extravasation dynamics of metastatic tumor cells, J. Cell Sci. 123 (2010) 2332–2341. doi:10.1242/jcs.069443.

[6] C.B. Kimmel, W.W. Ballard, S.R. Kimmel, B. Ullmann, T.F. Schilling, Stages of embryonic development of the zebrafish, Dev. Dyn. 203 (1995) 253–310. doi:10.1002/aja.1002030302.

[7] K. Howe, M.D. Clark, C.F. Torroja, J. Torrance, C. Berthelot, M. Muffato, J.E. Collins, S. Humphray, K. McLaren, L. Matthews, S. McLaren, I. Sealy, M. Caccamo, C. Churcher, C. Scott, J.C. Barrett, R. Koch, G.-J. Rauch, S. White, W. Chow, B. Kilian, L.T. Quintais, J.A. Guerra-Assunção, Y. Zhou, Y. Gu, J. Yen, J.-H. Vogel, T. Eyre, S. Redmond, R. Banerjee, J. Chi, B. Fu, E. Langley, S.F. Maguire, G.K. Laird, D. Lloyd, E. Kenyon, S. Donaldson, H. Sehra, J. Almeida-King, J. Loveland, S. Trevanion, M. Jones, M. Quail, D. Willey, A. Hunt, J. Burton, S. Sims, K. McLay, B. Plumb, J. Davis, C. Clee, K. Oliver, R. Clark, C. Riddle, D. Elliott, G. Threadgold, G. Harden, D. Ware, S. Begum, B. Mortimore, G. Kerry, P. Heath, B. Phillimore, A. Tracey, N. Corby, M. Dunn, C. Johnson, J. Wood, S. Clark, S. Pelan, G. Griffiths, M. Smith, R. Glithero, P. Howden, N. Barker, C. Lloyd, C. Stevens, J. Harley, K. Holt, G. Panagiotidis, J. Lovell, H. Beasley, C. Henderson, D. Gordon, K. Auger, D. Wright, J. Collins, C. Raisen, L. Dyer, K. Leung, L. Robertson, K. Ambridge, D. Leongamornlert, S. McGuire, R. Gilderthorp, C. Griffiths, D. Manthravadi, S. Nichol, G. Barker, S. Whitehead, M. Kay, J. Brown, C. Murnane, E. Gray, M. Humphries, N. Sycamore, D. Barker, D. Saunders, J. Wallis, A. Babbage, S. Hammond, M. Mashreghi-Mohammadi, L. Barr, S. Martin, P. Wray, A. Ellington, N. Matthews, M. Ellwood, R. Woodmansey, G. Clark, J.D. Cooper, A. Tromans, D. Grafham, C. Skuce, R. Pandian, R. Andrews, E. Harrison, A. Kimberley, J. Garnett, N. Fosker, R. Hall, P. Garner, D. Kelly, C. Bird, S. Palmer, I. Gehring, A. Berger, C.M. Dooley, Z. Ersan-Ürün, C. Eser, H. Geiger, M. Geisler, L. Karotki, A. Kirn, J. Konantz, M. Konantz, M.

Oberländer, S. Rudolph-Geiger, M. Teucke, C. Lanz, G. Raddatz, K. Osoegawa, B. Zhu, A. Rapp, S. Widaa, C. Langford, F. Yang, S.C. Schuster, N.P. Carter, J. Harrow, Z. Ning, J. Herrero, S.M.J. Searle, A. Enright, R. Geisler, R.H.A. Plasterk, C. Lee, M. Westerfield, P.J. de Jong, L.I. Zon, J.H. Postlethwait, C. Nüsslein-Volhard, T.J.P. Hubbard, H.R. Crollius, J. Rogers, D.L. Stemple, The zebrafish reference genome sequence and its relationship to the human genome, Nature. 496 (2013) 498–503. doi:10.1038/nature12111.

[8] J. Summerton, D. Weller, Morpholino Antisense Oligomers: Design, Preparation, and Properties, Antisense Nucleic Acid Drug Dev. 7 (1997) 187–195. doi:10.1089/oli.1.1997.7.187.

[9] W.Y. Hwang, Y. Fu, D. Reyon, M.L. Maeder, P. Kaini, J.D. Sander, J.K. Joung, R.T. Peterson, J.-R.J. Yeh, Heritable and Precise Zebrafish Genome Editing Using a CRISPR-Cas System, PLoS ONE. 8 (2013). doi:10.1371/journal.pone.0068708.

[10] L.M.J. Lee, E.A. Seftor, G. Bonde, R.A. Cornell, M.J.C. Hendrix, The fate of human malignant melanoma cells transplanted into zebrafish embryos: Assessment of migration and cell division in the absence of tumor formation, Dev. Dyn. 233 (2005) 1560–1570. doi:10.1002/dvdy.20471.

[11] M. Haldi, C. Ton, W.L. Seng, P. McGrath, Human melanoma cells transplanted into zebrafish proliferate, migrate, produce melanin, form masses and stimulate angiogenesis in zebrafish, Angiogenesis. 9 (2006) 139–151. doi:10.1007/s10456-006-9040-2.

[12] I.J. Marques, F.U. Weiss, D.H. Vlecken, C. Nitsche, J. Bakkers, A.K. Lagendijk, L.I. Partecke, C.-D. Heidecke, M.M. Lerch, C.P. Bagowski, Metastatic behaviour of primary human tumours in a zebrafish xenotransplantation model, BMC Cancer. 9 (2009) 128. doi:10.1186/1471-2407-9-128.

[13] D.P. Corkery, G. Dellaire, J.N. Berman, Leukaemia xenotransplantation in zebrafish – chemotherapy response assay in vivo, Br. J. Haematol. 153 (2011) 786–789. doi:10.1111/j.1365-2141.2011.08661.x.

[14] B. Pruvot, A. Jacquel, N. Droin, P. Auberger, D. Bouscary, J. Tamburini, M. Muller, M. Fontenay, J. Chluba, E. Solary, Leukemic cell xenograft in zebrafish embryo for investigating drug efficacy, Haematologica. 96 (2011) 612–616. doi:10.3324/haematol.2010.031401.

[15] K. Stoletov, R. Klemke, Catch of the day: zebrafish as a human cancer model, Oncogene. 27 (2008) 4509–4520. doi:10.1038/onc.2008.95.

[16] P. Cabezas-Sainz, J. Guerra-Varela, M.J. Carreira, J. Mariscal, M. Roel, J.A. Rubiolo, A.A. Sciara, M. Abal, L.M. Botana, R. López, L. Sánchez, Improving zebrafish embryo xenotransplantation conditions by increasing incubation temperature and establishing a proliferation index with ZFtool, BMC Cancer. 18 (2018). doi:10.1186/s12885-017-3919-8.

[17] S. Lal, J. La Du, R.L. Tanguay, J.A. Greenwood, Calpain 2 Is Required for the Invasion of Glioblastoma Cells in the Zebrafish Brain Microenvironment, J. Neurosci. Res. 90 (2012) 769–781. doi:10.1002/jnr.22794.

[18] C.J. Veinotte, G. Dellaire, J.N. Berman, Hooking the big one: the potential of zebrafish xenotransplantation to reform cancer drug screening in the genomic era, Dis. Model. Mech. 7 (2014) 745–754. doi:10.1242/dmm.015784.
[19] G. Hen, J. Nicenboim, O. Mayseless, L. Asaf, M. Shin, G. Busolin, R. Hofi, G. Almog, N. Tiso, N.D. Lawson, K. Yaniv, Venous-derived angioblasts generate organ-specific vessels during zebrafish embryonic development, Dev. Camb. Engl. 142 (2015) 4266–4278. doi:10.1242/dev.129247.
[20] B.S. Clark, M. Winter, A.R. Cohen, B.A. Link, Generation of Rab-based transgenic lines for in vivo studies of endosome biology in zebrafish, Dev. Dyn. Off. Publ. Am. Assoc. Anat. 240 (2011) 2452–2465. doi:10.1002/dvdy.22758.
[21] C. Norden, S. Young, B.A. Link, W.A. Harris, Actomyosin Is the Main Driver of Interkinetic Nuclear Migration in the Retina, Cell. 138 (2009) 1195–1208. doi:10.1016/j.cell.2009.06.032.
[22] M. Distel, J.C. Hocking, K. Volkmann, R.W. Köster, The centrosome neither persistently leads migration nor determines the site of axonogenesis in migrating neurons in vivo, J. Cell Biol. 191 (2010) 875–890. doi:10.1083/jcb.201004154.
[23] M. Jung Kim, K. Ho Kang, C.-H. Kim, S.-Y. Choi, Real-time imaging of mitochondria in transgenic zebrafish expressing mitochondrially targeted GFP, BioTechniques. 45 (2008) 331–334. doi:10.2144/000112909.
[24] X. Yang, W. Cui, A. Gu, C. Xu, S. Yu, T. Li, Y. Cui, X. Zhang, X. Bian, A Novel Zebrafish Xenotransplantation Model for Study of Glioma Stem Cell Invasion, PLoS ONE. 8 (2013) e61801. doi:10.1371/journal.pone.0061801.
[25] Y. Teng, X. Xie, S. Walker, D.T. White, J.S. Mumm, J.K. Cowell, Evaluating human cancer cell metastasis in zebrafish, BMC Cancer. 13 (2013) 453. doi:10.1186/1471-2407-13-453.
[26] S. Nicoli, M. Presta, The zebrafish/tumor xenograft angiogenesis assay, Nat. Protoc. 2 (2007) 2918–2923. doi:10.1038/nprot.2007.412.
[27] Y. Wang, M. Nakayama, M.E. Pitulescu, T.S. Schmidt, M.L. Bochenek, A. Sakakibara, S. Adams, A. Davy, U. Deutsch, U. Lüthi, A. Barberis, L.E. Benjamin, T. Mäkinen, C.D. Nobes, R.H. Adams, Ephrin-B2 controls VEGF-induced angiogenesis and lymphangiogenesis, Nature. 465 (2010) 483–486. doi:10.1038/nature09002.
[28] T.A. Martin, L. Ye, A.J. Sanders, J. Lane, W.G. Jiang, Cancer Invasion and Metastasis: Molecular and Cellular Perspective, Landes Bioscience, 2013. https://www.ncbi.nlm.nih.gov/books/NBK164700/ (accessed December 5, 2016).
[29] L. Hamilton, K.R. Astell, G. Velikova, D. Sieger, A Zebrafish Live Imaging Model Reveals Differential Responses of Microglia Toward Glioblastoma Cells In Vivo, Zebrafish. 13 (2016) 523–534. doi:10.1089/zeb.2016.1339.
[30] K.M. Wiens, H.L. Lee, H. Shimada, A.E. Metcalf, M.Y. Chao, C.-L. Lien, Platelet-Derived Growth Factor Receptor β Is Critical for Zebrafish Intersegmental Vessel Formation, PLoS ONE. 5 (2010). doi:10.1371/journal.pone.0011324.

[31] A.C. Bellail, S.B. Hunter, D.J. Brat, C. Tan, E.G. Van Meir, Microregional extracellular matrix heterogeneity in brain modulates glioma cell invasion, Int. J. Biochem. Cell Biol. 36 (2004) 1046–1069. doi:10.1016/j.biocel.2004.01.013.
[32] Y. Wang, L. Pan, C.B. Moens, B. Appel, Notch3 establishes brain vascular integrity by regulating pericyte number, Dev. Camb. Engl. 141 (2014) 307–317. doi:10.1242/dev.096107.
[33] K. Paňková, D. Rösel, M. Novotný, J. Brábek, The molecular mechanisms of transition between mesenchymal and amoeboid invasiveness in tumor cells, Cell. Mol. Life Sci. 67 (2010) 63–71. doi:10.1007/s00018-009-0132-1.
[34] G.R. Garcia, P.D. Noyes, R.L. Tanguay, Advancements in zebrafish applications for 21st century toxicology, Pharmacol. Ther. 161 (2016) 11–21. doi:10.1016/j.pharmthera.2016.03.009.
[35] N. Irie, S. Kuratani, Comparative transcriptome analysis reveals vertebrate phylotypic period during organogenesis, Nat. Commun. 2 (2011) 248. doi:10.1038/ncomms1248.
[36] L. Truong, S.L. Harper, R.L. Tanguay, Evaluation of Embryotoxicity Using the Zebrafish Model, in: Drug Saf. Eval., Humana Press, 2011: pp. 271–279. doi:10.1007/978-1-60761-849-2_16.
[37] M.C. Mione, N.S. Trede, The zebrafish as a model for cancer, Dis. Model. Mech. 3 (2010) 517–523. doi:10.1242/dmm.004747.
[38] J.K. Leet, C.D. Lindberg, L.A. Bassett, G.M. Isales, K.L. Yozzo, T.D. Raftery, D.C. Volz, High-Content Screening in Zebrafish Embryos Identifies Butafenacil as a Potent Inducer of Anemia, PLOS ONE. 9 (2014) e104190. doi:10.1371/journal.pone.0104190.
[39] R. Liu, S. Lin, R. Rallo, Y. Zhao, R. Damoiseaux, T. Xia, S. Lin, A. Nel, Y. Cohen, Automated Phenotype Recognition for Zebrafish Embryo Based In Vivo High Throughput Toxicity Screening of Engineered Nano-Materials, PLOS ONE. 7 (2012) e35014. doi:10.1371/journal.pone.0035014.
[40] V.L. Bentley, C.J. Veinotte, D.P. Corkery, J.B. Pinder, M.A. LeBlanc, K. Bedard, A.P. Weng, J.N. Berman, G. Dellaire, Focused chemical genomics using zebrafish xenotransplantation as a pre-clinical therapeutic platform for T-cell acute lymphoblastic leukemia, Haematologica. 100 (2015) 70–76. doi:10.3324/haematol.2014.110742.
[41] P. Diehr, D.C. Martin, T. Koepsell, A. Cheadle, Breaking the matches in a paired t-test for community interventions when the number of pairs is small, Stat. Med. 14 (1995) 1491–1504. doi:10.1002/sim.4780141309.
[42] L.C. Wehmas, R.L. Tanguay, A. Punnoose, J.A. Greenwood, Developing a Novel Embryo-Larval Zebrafish Xenograft Assay to Prioritize Human Glioblastoma Therapeutics, Zebrafish. 13 (2016) 317–329. doi:10.1089/zeb.2015.1170.
[43] G.P. Gupta, J. Massagué, Cancer Metastasis: Building a Framework, Cell. 127 (2006) 679–695. doi:10.1016/j.cell.2006.11.001.
[44] X. Xie, S.-C. Tang, Y. Cai, W. Pi, L. Deng, G. Wu, A. Chavanieu, Y. Teng, Suppression of breast cancer metastasis through the inactivation of ADP-ribosylation factor 1, Oncotarget. 7 (2016) 58111–58120. doi:10.18632/oncotarget.11185.

[45] C. Raimondi, V. Calleja, R. Ferro, A. Fantin, A.M. Riley, B.V.L. Potter, C.H. Brennan, T. Maffucci, B. Larijani, M. Falasca, A Small Molecule Inhibitor of PDK1/PLCγ1 Interaction Blocks Breast and Melanoma Cancer Cell Invasion, Sci. Rep. 6 (2016) 26142. doi:10.1038/srep26142.

[46] J. Chen, W. Zhou, Q. Jia, J. Chen, S. Zhang, W. Yao, F. Wei, Y. Zhang, F. Yang, W. Huang, Y. Zhang, H. Zhang, Y. Zhang, B. Huang, Z. Zhang, H. Jia, N. Wang, Efficient extravasation of tumor-repopulating cells depends on cell deformability, Sci. Rep. 6 (2016) 19304. doi:10.1038/srep19304.

[47] R. Pulak, Tools for automating the imaging of zebrafish larvae, Methods. 96 (2016) 118–126. doi:10.1016/j.ymeth.2015.11.021.

[48] R. Beer, G. Franz, S. Krajewski, B.R. Pike, R.L. Hayes, J.C. Reed, K.K. Wang, C. Klimmer, E. Schmutzhard, W. Poewe, A. Kampfl, Temporal and spatial profile of caspase 8 expression and proteolysis after experimental traumatic brain injury: Caspase 8 expression and proteolysis after TBI, J. Neurochem. 78 (2001) 862–873. doi:10.1046/j.1471-4159.2001.00460.x.

[49] G. Franz, R. Beer, D. Intemann, S. Krajewski, J.C. Reed, K. Engelhardt, B.R. Pike, R.L. Hayes, K.K. Wang, E. Schmutzhard, A. Kampfl, Temporal and Spatial Profile of Bid Cleavage after Experimental Traumatic Brain Injury, J. Cereb. Blood Flow Metab. 22 (2002) 951–958. doi:10.1097/00004647-200208000-00006.

[50] N. Kyprianou, J.T. Isaacs, Activation of Programmed Cell Death in the Rat Ventral Prostate after Castration, Endocrinology. 122 (1988) 552–562. doi:10.1210/endo-122-2-552.

[51] P. Friedl, S. Alexander, Cancer Invasion and the Microenvironment: Plasticity and Reciprocity, Cell. 147 (2011) 992–1009. doi:10.1016/j.cell.2011.11.016.

[52] A.M. Welker, B.D. Jaros, V.K. Puduvalli, J. Imitola, B. Kaur, C.E. Beattie, Standardized orthotopic xenografts in zebrafish reveal glioma cell-line-specific characteristics and tumor cell heterogeneity, Dis. Model. Mech. 9 (2016) 199–210. doi:10.1242/dmm.022921.

[53] U. Linz, Commentary on effects of radiotherapy with concomitant and adjuvant temozolomide versus radiotherapy alone on survival in glioblastoma in a randomised phase III study: 5-Year analysis of the EORTC-NCIC trial (Lancet Oncol. 2009;10:459-466), Cancer. 116 (2010) 1844–1846. doi:10.1002/cncr.24950.

[54] K. Ogura, T. Mizowaki, Y. Arakawa, M. Ogura, K. Sakanaka, S. Miyamoto, M. Hiraoka, Initial and cumulative recurrence patterns of glioblastoma after temozolomide-based chemoradiotherapy and salvage treatment: a retrospective cohort study in a single institution, Radiat. Oncol. Lond. Engl. 8 (2013) 97. doi:10.1186/1748-717X-8-97.

[55] Z.-C. Ye, H. Sontheimer, Glioma Cells Release Excitotoxic Concentrations of Glutamate, Cancer Res. 59 (1999) 4383–4391.

[56] M. Aumailley, The laminin family, Cell Adhes. Migr. 7 (2013) 48–55. doi:10.4161/cam.22826.

[57] S. Watkins, S. Robel, I.F. Kimbrough, S.M. Robert, G. Ellis-Davies, H. Sontheimer, Disruption of astrocyte–vascular coupling and the blood–brain

barrier by invading glioma cells, Nat. Commun. 5 (2014) ncomms5196. doi:10.1038/ncomms5196.

[58] R. Hallmann, N. Horn, M. Selg, O. Wendler, F. Pausch, L.M. Sorokin, Expression and Function of Laminins in the Embryonic and Mature Vasculature, Physiol. Rev. 85 (2005) 979–1000. doi:10.1152/physrev.00014.2004.

[59] T. Kawataki, T. Yamane, H. Naganuma, P. Rousselle, I. Andurén, K. Tryggvason, M. Patarroyo, Laminin isoforms and their integrin receptors in glioma cell migration and invasiveness: Evidence for a role of α5-laminin(s) and α3β1 integrin, Exp. Cell Res. 313 (2007) 3819–3831. doi:10.1016/j.yexcr.2007.07.038.

[60] N. Pouliot, N. Kusuma, Laminin-511: A multi-functional adhesion protein regulating cell migration, tumor invasion and metastasis, Cell Adhes. Migr. 7 (2013) 142–149. doi:10.4161/cam.22125.

[61] Y. Kikkawa, T. Ogawa, R. Sudo, Y. Yamada, F. Katagiri, K. Hozumi, M. Nomizu, J.H. Miner, The Lutheran/Basal Cell Adhesion Molecule Promotes Tumor Cell Migration by Modulating Integrin-mediated Cell Attachment to Laminin-511 Protein, J. Biol. Chem. 288 (2013) 30990–31001. doi:10.1074/jbc.M113.486456.

[62] N. Kusuma, R.L. Anderson, N. Pouliot, Laminin α5-derived peptides modulate the properties of metastatic breast tumour cells, Clin. Exp. Metastasis. 28 (2011) 909–921. doi:10.1007/s10585-011-9422-8.

[63] C.A. MacRae, R.T. Peterson, Zebrafish as tools for drug discovery, Nat. Rev. Drug Discov. 14 (2015) 721–731. doi:10.1038/nrd4627.

[64] E. Delamarre, S. Taboubi, S. Mathieu, C. Berenguer, V. Rigot, J.-C. Lissitzky, D. Figarella-Branger, L. Ouafik, J. Luis, Expression of Integrin α6β1 Enhances Tumorigenesis in Glioma Cells, Am. J. Pathol. 175 (2009) 844–855. doi:10.2353/ajpath.2009.080920.

[65] A.E. Webb, J. Sanderford, D. Frank, W.S. Talbot, W. Driever, D. Kimelman, Laminin α5 is essential for the formation of the zebrafish fins, Dev. Biol. 311 (2007) 369–382. doi:10.1016/j.ydbio.2007.08.034.

[66] J. Schindelin, I. Arganda-Carreras, E. Frise, V. Kaynig, M. Longair, T. Pietzsch, S. Preibisch, C. Rueden, S. Saalfeld, B. Schmid, J.-Y. Tinevez, D.J. White, V. Hartenstein, K. Eliceiri, P. Tomancak, A. Cardona, Fiji: an open-source platform for biological-image analysis, Nat. Methods. 9 (2012) 676–682. doi:10.1038/nmeth.2019.

[67] J. Ollion, J. Cochennec, F. Loll, C. Escudé, T. Boudier, TANGO: a generic tool for high-throughput 3D image analysis for studying nuclear organization, Bioinformatics. 29 (2013) 1840–1841. doi:10.1093/bioinformatics/btt276.

[68] N. Otsu, A Threshold Selection Method from Gray-Level Histograms, IEEE Trans. Syst. Man Cybern. 9 (1979) 62–66. doi:10.1109/TSMC.1979.4310076.

[69] G.W. Zack, W.E. Rogers, S.A. Latt, Automatic measurement of sister chromatid exchange frequency., J. Histochem. Cytochem. 25 (1977) 741–753. doi:10.1177/25.7.70454.

[70] S. Bolte, F.P. Cordelières, A guided tour into subcellular colocalization analysis in light microscopy, J. Microsc. 224 (2006) 213–232. doi:10.1111/j.1365-2818.2006.01706.x.
[71] A. Parslow, A. Cardona, R.J. Bryson-Richardson, Sample Drift Correction Following 4D Confocal Time-lapse Imaging, J. Vis. Exp. JoVE. (2014). doi:10.3791/51086.
[72] N. Kusuma, D. Denoyer, J.A. Eble, R.P. Redvers, B.S. Parker, R. Pelzer, R.L. Anderson, N. Pouliot, Integrin-dependent response to laminin-511 regulates breast tumor cell invasion and metastasis, Int. J. Cancer. 130 (2012) 555–566. doi:10.1002/ijc.26018.
[73] Y. Piao, J. Liang, L. Holmes, V. Henry, E. Sulman, J.F. de Groot, Acquired Resistance to Anti-VEGF Therapy in Glioblastoma Is Associated with a Mesenchymal Transition, Clin. Cancer Res. 19 (2013) 4392–4403. doi:10.1158/1078-0432.CCR-12-1557.
[74] K.V. Lu, J.P. Chang, C.A. Parachoniak, M.M. Pandika, M.K. Aghi, D. Meyronet, N. Isachenko, S.D. Fouse, J.J. Phillips, D.A. Cheresh, M. Park, G. Bergers, VEGF Inhibits Tumor Cell Invasion and Mesenchymal Transition Through a MET/VEGFR2 Complex, Cancer Cell. 22 (2012) 21–35. doi:10.1016/j.ccr.2012.05.037.
[75] T. Kessler, F. Sahm, J. Blaes, M. Osswald, P. Rübmann, D. Milford, S. Urban, L. Jestaedt, S. Heiland, M. Bendszus, A. Hertenstein, P.-N. Pfenning, C.R. de Almodóvar, A. Wick, F. Winkler, A. von Deimling, M. Platten, W. Wick, M. Weiler, Glioma cell VEGFR-2 confers resistance to chemotherapeutic and antiangiogenic treatments in PTEN-deficient glioblastoma, Oncotarget. 6 (2015) 31050–31068.
[76] S.K. Gopal, D.W. Greening, H.-J. Zhu, R.J. Simpson, R.A. Mathias, Transformed MDCK cells secrete elevated MMP1 that generates LAMA5 fragments promoting endothelial cell angiogenesis, Sci. Rep. 6 (2016). doi:10.1038/srep28321.
[77] J.-Y. Tinevez, N. Perry, J. Schindelin, G.M. Hoopes, G.D. Reynolds, E. Laplantine, S.Y. Bednarek, S.L. Shorte, K.W. Eliceiri, TrackMate: An open and extensible platform for single-particle tracking, Methods. (n.d.). doi:10.1016/j.ymeth.2016.09.016.
[78] P.E. Czabotar, G. Lessene, A. Strasser, J.M. Adams, Control of apoptosis by the BCL-2 protein family: implications for physiology and therapy, Nat. Rev. Mol. Cell Biol. 15 (2014) 49–63. doi:10.1038/nrm3722.
[79] K.W. Yip, J.C. Reed, Bcl-2 family proteins and cancer, Oncogene. 27 (2008) 6398–6406. doi:10.1038/onc.2008.307.
[80] S.A. Amundson, T.G. Myers, D. Scudiero, S. Kitada, J.C. Reed, A.J. Fornace, An Informatics Approach Identifying Markers of Chemosensitivity in Human Cancer Cell Lines, Cancer Res. 60 (2000) 6101–6110.
[81] C. Teixeira, J.C. Reed, M.A.C. Pratt, Estrogen Promotes Chemotherapeutic Drug Resistance by a Mechanism Involving Bcl-2 Proto-Oncogene Expression in Human Breast Cancer Cells, Cancer Res. 55 (1995) 3902–3907.
[82] S.K. Kolluri, N. Bruey-Sedano, X. Cao, B. Lin, F. Lin, Y.-H. Han, M.I. Dawson, X. Zhang, Mitogenic Effect of Orphan Receptor TR3 and Its

Regulation by MEKK1 in Lung Cancer Cells, Mol. Cell. Biol. 23 (2003) 8651–8667. doi:10.1128/MCB.23.23.8651-8667.2003.

[83] B. Lin, S.K. Kolluri, F. Lin, W. Liu, Y.-H. Han, X. Cao, M.I. Dawson, J.C. Reed, X. Zhang, Conversion of Bcl-2 from Protector to Killer by Interaction with Nuclear Orphan Receptor Nur77/TR3, Cell. 116 (2004) 527–540. doi:10.1016/S0092-8674(04)00162-X.

[84] X. Zhang, Targeting Nur77 translocation, Expert Opin. Ther. Targets. 11 (2007) 69–79. doi:10.1517/14728222.11.1.69.

[85] U.M. Moll, N. Marchenko, X.–. Zhang, p53 and Nur77/TR3 – transcription factors that directly target mitochondria for cell death induction, Oncogene. 25 (2006) 4725–4743. doi:10.1038/sj.onc.1209601.

[86] T.M. Allen, Ligand-targeted therapeutics in anticancer therapy, Nat. Rev. Cancer. 2 (2002) 750–763. doi:10.1038/nrc903.

[87] S.K. Kolluri, X. Zhu, X. Zhou, B. Lin, Y. Chen, K. Sun, X. Tian, J. Town, X. Cao, F. Lin, D. Zhai, S. Kitada, F. Luciano, E. Donnell, Y. Cao, F. He, J. Lin, J.C. Reed, A.C. Satterthwait, X. Zhang, A Short Nur77-derived Peptide Converts Bcl-2 from a Protector to a Killer, Cancer Cell. 14 (2008) 285–298. doi:10.1016/j.ccr.2008.09.002.

[88] Y.-F. Xiao, M.-M. Jie, B.-S. Li, C.-J. Hu, R. Xie, B. Tang, S.-M. Yang, Peptide-Based Treatment: A Promising Cancer Therapy, J. Immunol. Res. 2015 (2015). doi:10.1155/2015/761820.

[89] T. Liu, J. Tian, Z. Chen, Y. Liang, J. Liu, S. Liu, H. Li, J. Zhan, X. Yang, Anti-TROP2 conjugated hollow gold nanospheres as a novel nanostructure for targeted photothermal destruction of cervical cancer cells, Nanotechnology. 25 (2014) 345103. doi:10.1088/0957-4484/25/34/345103.

[90] C. Xiong, W. Lu, M. Zhou, X. Wen, C. Li, Cisplatin-loaded hollow gold nanoparticles for laser-triggered release, Cancer Nanotechnol. 9 (2018). doi:10.1186/s12645-018-0041-9.

[91] G. Itchaki, J.R. Brown, The potential of venetoclax (ABT-199) in chronic lymphocytic leukemia, Ther. Adv. Hematol. 7 (2016) 270–287. doi:10.1177/2040620716655350.

[92] K.A. Rogers, J.C. Byrd, Venetoclax Adds a New Arrow Targeting Relapsed CLL to the Quiver, Cancer Cell. 29 (2016) 3–4. doi:10.1016/j.ccell.2015.12.010.

[93] S.K. Tahir, M.L. Smith, P. Hessler, L.R. Rapp, K.B. Idler, C.H. Park, J.D. Leverson, L.T. Lam, Potential mechanisms of resistance to venetoclax and strategies to circumvent it, BMC Cancer. 17 (2017). doi:10.1186/s12885-017-3383-5.

[94] I. Kola, J. Landis, Can the pharmaceutical industry reduce attrition rates?, Nat. Rev. Drug Discov. 3 (2004) 711–716. doi:10.1038/nrd1470.

[95] S.H. Lam, H.L. Chua, Z. Gong, T.J. Lam, Y.M. Sin, Development and maturation of the immune system in zebrafish, Danio rerio: a gene expression profiling, in situ hybridization and immunological study, Dev. Comp. Immunol. 28 (2004) 9–28. doi:10.1016/S0145-305X(03)00103-4.

[96] M. Konantz, T.B. Balci, U.F. Hartwig, G. Dellaire, M.C. André, J.N. Berman, C. Lengerke, Zebrafish xenografts as a tool for in vivo studies on human

cancer, Ann. N. Y. Acad. Sci. 1266 (2012) 124–137. doi:10.1111/j.1749-6632.2012.06575.x.
[97] C. Santoriello, L.I. Zon, Hooked! Modeling human disease in zebrafish, J. Clin. Invest. 122 (2012) 2337–2343. doi:10.1172/JCI60434.
[98] H. Li, C.E. Nelson, B.C. Evans, C.L. Duvall, Delivery of Intracellular-acting Biologics in Pro-Apoptotic Therapies, Curr. Pharm. Des. 17 (2011) 293–319.
[99] V. Krishnan, A.K. Rajasekaran, Clinical Nanomedicine: A Solution to the Chemotherapy Conundrum in Pediatric Leukemia Therapy, Clin. Pharmacol. Ther. 95 (2014) 168–178. doi:10.1038/clpt.2013.174.
[100] W.J. Gradishar, S. Tjulandin, N. Davidson, H. Shaw, N. Desai, P. Bhar, M. Hawkins, J. O'Shaughnessy, Phase III Trial of Nanoparticle Albumin-Bound Paclitaxel Compared With Polyethylated Castor Oil–Based Paclitaxel in Women With Breast Cancer, J. Clin. Oncol. 23 (2005) 7794–7803. doi:10.1200/JCO.2005.04.937.
[101] L. Mercatali, F. La Manna, A. Groenewoud, R. Casadei, F. Recine, G. Miserocchi, F. Pieri, C. Liverani, A. Bongiovanni, C. Spadazzi, A. de Vita, G. van der Pluijm, A. Giorgini, R. Biagini, D. Amadori, T. Ibrahim, E. Snaar-Jagalska, Development of a Patient-Derived Xenograft (PDX) of Breast Cancer Bone Metastasis in a Zebrafish Model, Int. J. Mol. Sci. 17 (2016). doi:10.3390/ijms17081375.
[102] R.J. Petrie, K.M. Yamada, At the leading edge of three-dimensional cell migration, J. Cell Sci. 125 (2012) 5917–5926. doi:10.1242/jcs.093732.
[103] T.-L. Liu, S. Upadhyayula, D.E. Milkie, V. Singh, K. Wang, I.A. Swinburne, K.R. Mosaliganti, Z.M. Collins, T.W. Hiscock, J. Shea, A.Q. Kohrman, T.N. Medwig, D. Dambournet, R. Forster, B. Cunniff, Y. Ruan, H. Yashiro, S. Scholpp, E.M. Meyerowitz, D. Hockemeyer, D.G. Drubin, B.L. Martin, D.Q. Matus, M. Koyama, S.G. Megason, T. Kirchhausen, E. Betzig, Observing the cell in its native state: Imaging subcellular dynamics in multicellular organisms, Science. 360 (2018) eaaq1392. doi:10.1126/science.aaq1392.
[104] C.S. von Bartheld, F.S. Wouters, Quantitative Techniques for Imaging Cells and Tissues, Cell Tissue Res. 360 (2015) 1–4. doi:10.1007/s00441-015-2149-0.
[105] E. Kreit, L.M. Mäthger, R.T. Hanlon, P.B. Dennis, R.R. Naik, E. Forsythe, J. Heikenfeld, Biological versus electronic adaptive coloration: how can one inform the other?, J. R. Soc. Interface. (2012) rsif20120601. doi:10.1098/rsif.2012.0601.